Residual stress and its role in failure

P J Withers

School of Materials, University of Manchester, Grosvenor St., Manchester, M1 7HS, UK

E-mail: philip.withers@manchester.ac.uk

Abstract

Our safety, comfort and peace of mind are heavily dependent upon our capability to prevent, predict or postpone the failure of components and structures on the basis of sound physical principles. While the external loadings acting on a material or component are clearly important, There are other contributory factors including unfavourable materials microstructure, pre-existing defects and residual stresses. Residual stresses can add to, or subtract from, the applied stresses and so when unexpected failure occurs it is often because residual stresses have combined critically with the applied stresses, or because together with the presence of undetected defects they have dangerously lowered the applied stress at which failure will occur. Consequently it is important that the origins of residual stress are understood, opportunities for removing harmful or introducing beneficial residual stresses recognized, their evolution in-service predicted, their influence on failure processes understood and safe structural integrity assessments made, so as to either remove the part prior to failure, or to take corrective action to extend life. This paper reviews the progress in these aspects in the light of the basic failure mechanisms.

(Some figures in this article are in colour only in the electronic version)

Contents

1. Introduction

The prediction, prevention or postponement of failure in components and structures upon the basis of sound physics is not just an interesting topic for research, but is essential for the safe execution of our daily lives (James 1998, Miller 2003). There are many ways in which failure can occur including brittle fracture, plastic collapse, fatigue, creep and stress corrosion cracking. While the external loadings acting on a material or component are clearly important, other factors often play a determining role. In fact when predicting whether and when failure will occur it is often the case that the external loading is the most easily considered factor. Other contributory factors include unfavourable microstructure, the likelihood of pre-existing defects and residual stresses. The science of fracture mechanics was established to apply the theories of elasticity and plasticity, to consider the effect of microscopic defects and thereby to predict the macroscopic strength and failure mode. Compared with the role of defects, the role of residual stress on failure has received relatively little attention. This probably reflects historical difficulties associated with their measurement and prediction. Their prediction *a priori* is difficult because they are a product of almost every processing stage in manufacturing and subsequently evolve during life in-service. Their measurement is hampered by the fact that they leave no outward sign. They can add to, or subtract from, stresses applied during service. Consequently, when unexpected failure occurs it is often because residual stresses have combined critically with the applied stresses, or because they, together with the presence of unknown defects or poor microstucture, have dangerously lowered the stress at which failure will occur.

In view of the above, it is clearly important that the origins of residual stress are recognized, means for predicting their evolution in-service developed, and their influence on failure processes understood. In this way residual stresses can be incorporated into safe structural integrity assessments, leading either to removal of the part prior to failure, or to corrective reparative action when necessary. This review is intended to provide an overview for physical scientists of the current understanding of residual stresses, including methods for their measurement and prediction. Given that the physical mechanisms underpinning the fracture and strength of solids have not been reviewed in this journal since the excellent paper by Orowan (1948) and much has happened in the interim, the basic foundations of modern fracture mechanics are briefly introduced on the way to examining the effect of residual stress on different failure mechanisms.

2. Basic principles of residual stress

2.1. Eigenstrains

Residual stresses are those stresses which are retained within a body when no external forces are acting. Residual stresses arise because of misfits (incompatibilities) between different regions of the material, component or assembly. Perhaps the simplest residual stress field is that due to an oversized sphere placed inside a spherical cavity in a large homogeneous body of the same material. This might occur by cooling a body containing a sphere having a smaller coefficient of thermal expansion, but the same elastic constants. For solely elastic accommodation, the included sphere experiences uniform residual compression and the stress in the matrix falls off with distance, r, from the centre of the sphere according to $1/r^3$. The solution to this particular problem was solved by Lamé in 1862. Eshelby (1957) developed a more general formulation, the solution of which describes the residual stress arising from the placement of an arbitrarily misfitting inclusion, Ω, having the same elastic constants as the

matrix. This approach can be generalized to describe any residual stress field by considering it as arising from a distribution of inelastic strains within the sample. In essence this is rather like superimposing the stress fields arising from a continuous distribution of infinitesimal point sources, each behaving like anisotropically misfitting spheres. This distribution of inelastic strain $\varepsilon_{kl}^*(\boldsymbol{x})$ is often termed the eigenstrain distribution (Mura 1987) and relates directly to the overall residual stress $\sigma_{ij}(\boldsymbol{x})$ or elastic strain:

$$\sigma_{ij}(\boldsymbol{x}) = -C_{ijkl}\left\{\int_{-\infty}^{\infty} C_{pqmn}\varepsilon_{mn}^*(\boldsymbol{x}')G_{kp,ql}(\boldsymbol{x}-\boldsymbol{x}')\,\mathrm{d}x' + \varepsilon_{kl}^*(\boldsymbol{x})\right\}. \tag{1}$$

Here C_{ijkl} are the elastic stiffness coefficients, and the Green's function $G_{kp}(\boldsymbol{x}-\boldsymbol{x}')$ represents the displacement component in the k direction at $\boldsymbol{x}$ when a body force is applied at $\boldsymbol{x}'$ in the p direction in an infinitely extended material ($G_{ij,l}(\boldsymbol{x}-\boldsymbol{x}') = \partial/\partial x_l.(G_{ij}(\boldsymbol{x}-\boldsymbol{x}'))$). For any field location x the integration in terms of x' needs to be carried out only over the misfitting region. (i.e. where the eigenstrain is non-zero). Using (1) it is relatively straightforward to calculate the residual stress field that arises for a given eigenstrain; this represents the forward problem. However, in practice a solution to the much more difficult inverse problem is often desired; namely, we would like to infer the underlying eigenstrain distribution from an incomplete (since they are determined only at a finite number of points with associated measurement errors) knowledge of the residual elastic strains or residual stresses (Korsunsky *et al* 2004, Ueda and Yuan 1993). Once a suitable eigenstrain distribution has been found, the *complete* residual stress field can be reconstructed through the solution of the *forward* problem. Most importantly, a knowledge of the eigenstrain distribution fully characterizes the residual stress field allowing its evolution to be predicted, for example as a result of material removal, crack propagation or heat treatment. Since residual stresses are self-equilibrating, the basic physical laws of solid mechanics demand stress and moment balance of residual stress everywhere within the body.

2.2. Classifications of residual stress

Residual stresses can be classified according to the manner in which they arise (e.g. Withers and Bhadeshia 2001), the scale over which they equilibrate (e.g. Noyan and Cohen 1987), or their effect on behaviour (e.g. Bouchard and Withers 2006). The misfits that cause residual stresses can be introduced in many ways. Perhaps the most common origins are non-uniform plastic flow, steep thermal gradients and phase transformations as indicated in figure 1.

Across any section through the body the component of the residual stresses normal to the section must balance; the length over which they do so in any direction is defined as the characteristic length, l_o. From a measurement perspective, the residual stress component is classified according to three characteristic length scales. Continuum level stresses that neglect the underlying microstructure are defined as type I stresses. Typically they equilibrate over a length scale comparable to the extent of the component, or structure, in that direction and are also termed macrostresses. These might arise from plastic bending of a bar for example (as shown in figures 1 and 11). While for microelectronic machines, electronic devices as well as for long cracks in engineering components, the length scale of these stresses can be very small, the key point is that they can be described by continuum mechanics. Microstructurally related stresses that equilibrate on a scale of a few grain diameters are generally termed intergranular stresses or type II microstresses; these tend to arise from inhomogeneity at the grain scale, for example from differences in slip behaviour from grain to grain. At a finer scale still are type III microstresses arising from heterogeneous behaviour at the atomic scale, these
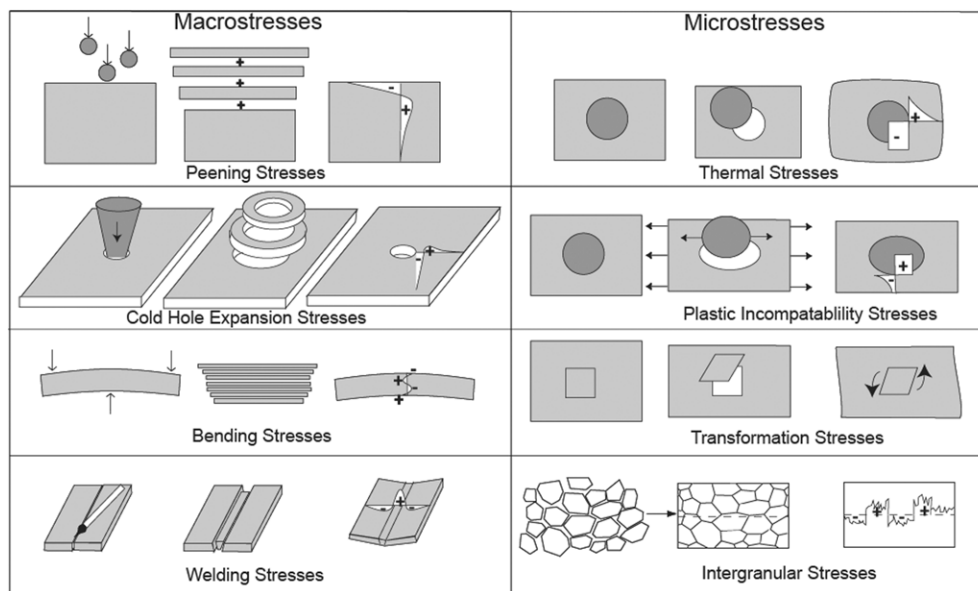
Figure 1. Residual stresses arise from misfits, either between different regions of a material or between different phases within the material. Examples of different types of residual macro- and micro-residual stress are illustrated schematically. In each case the process is indicated on the left, the misfit in the centre and the resulting stress pattern on the right-hand side (Withers and Bhadeshia 2001).

might arise from line defects (dislocations), point defects such as might arise from radiation damage or doping with atoms of a different size.

While the misfit may arise at a particular scale, the occurrence of many misfits at that scale may have a cumulative effect such that they give rise to stresses at a longer scale. For example, a single edge dislocation inserts a half-plane of atoms into a crystal creating a very local type III stress field, while the stress free shapes of the grains in a polycrystal are altered by the passage of many dislocations through their interior on differently oriented slip-planes causing type II intergranular misfit stresses as they are constrained by one another (figure 1). At a larger scale still, the cumulative presence of many geometrically necessary dislocations (Ashby 1970) can give rise to plastic strain gradients and thereby macroscale misfits and stresses of type I. In a glass type II stresses cannot arise. Here the doping of a glass surface with one K atom creates a type III microstress, but multiple ion exchange using molten salt baths introduces many atoms into the near surface region leading to substantial long-range compressive stress in-plane (Kistler 1962, Matthew *et al* 2003).

The average stress in each phase of a composite can have many of the characteristics of a long-range stress field, while being a microscale effect. To illustrate this type of residual stress consider the cooling of a matrix (phase 1) containing a single inclusion of another phase (phase 2). Except in the unlikely event that the two phases had the same coefficients of thermal expansion, this would create a type II stress. For a single spherical inclusion the stress field is that derived by Lamé (section 2.1). The stress field is essentially insignificant beyond a few particle diameters from the inclusion. However, if the matrix contains many inclusions of phase 2 then the stress normal to a plane would self-equilibrate over areas larger than some characteristic size, A_o. But it is not possible to measure the stresses over an area, except at a free surface where the residual stress normal to the surface is zero by definition. Integrating over
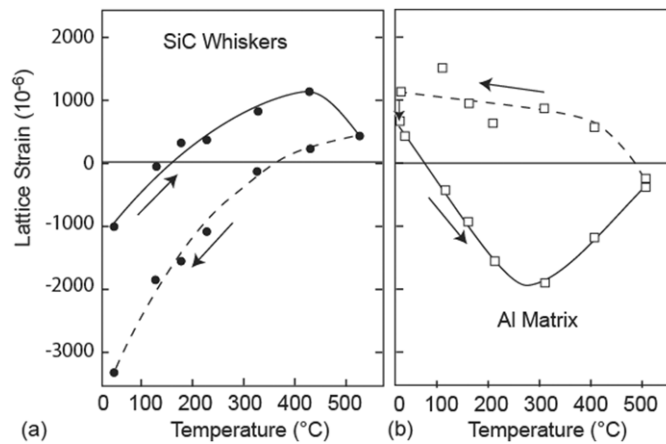
Figure 2. Neutron strain measurements of the mean Al and SiC longitudinal 111 lattice strain components in (*a*) the aligned whiskers, and (*b*) the matrix, for an Al/5%SiC$_W$, composite monitored over a thermal cycle. The arrows show the heating (solid) and cooling (dashed) curves (Withers *et al* 1987).

a characteristic sampling volume V_o large enough to include representative volume fractions (f_1 and f_2) of each phase (Noyan and Cohen 1987)

$$\int_{V_o} \sigma_1(x, y, z)\, \mathrm{d}V_1 + \sigma_2(x, y, z)\, \mathrm{d}V_2 = f_1 \langle \sigma_1 \rangle + f_2 \langle \sigma_2 \rangle = 0, \tag{2}$$

where $\langle \sigma_1 \rangle$ and $\langle \sigma_2 \rangle$ are termed mean phase microstresses by the present author (Withers 1988, Hutchings *et al* 2005). Since the total stress averages to zero over macroscopic length scales, the stress is correctly classified as a type II stress field and would be invisible to destructive stress measurement techniques. However, the average stresses in the two phases would be non-zero, being compressive in one and tensile in the other. Consequently, methods, such as diffraction techniques, which sample just one phase would measure a tensile or compressive stress even if the evaluation volume was greater than V_o. As a result they are sometimes mistaken for macrostresses when measuring stress by diffraction (even being termed pseudo-macrostresses (Cullity 1978)). A good example of this effect is provided by the elastic strains that arise as a two phase composite is heated/cooled (Saigal *et al* 1992, Withers 1995) as illustrated in figure 2.

All too often those making stress measurements have failed to consider what length scales and types of residual stress are important from a materials or component performance viewpoint. Unwittingly this can lead to inappropriate measurements and interpretations.

From a physics viewpoint, it is conceptually satisfying to consider the whole three dimensional stress field within a component, as well as the internal misfits (eigenstrains) and externally applied constraints from which they arise. From such a complete knowledge of the system it is then relatively simple to determine how the component responds and the stresses redistribute if the conditions are changed. However, such detailed information about the whole system can be costly or impractical to obtain. Engineers therefore often concentrate on the stress field local to a region of interest (sub-domain) and try to determine its effect on known or postulated defects (cracks, voids, etc) in the sub-domain. They have found it useful, from a structural integrity assessment viewpoint, to decompose the residual stress profile across a region of concern into membrane (i.e. the uniformly distributed stress giving the same integrated force, f over the sub-domain), σ_m, through-section bending, σ_b, relating to the
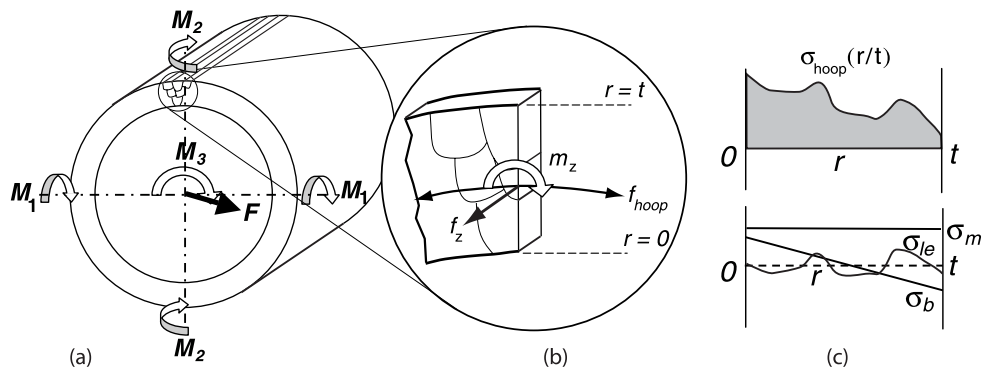
Figure 3. (*a*) By definition the net force, *F*, and moments (M_1, M_2, M_3) over any cut plane arising from a residual stress field must balance as shown here for a seam welded pipe, (*b*) the force and moments need not balance however within a sub-domain of interest (where a crack might arise for example), (*c*) here the hoop stress field acting on the wall section can be decomposed into the membrane, bending and locally equilibrating components after (Bouchard and Withers 2006).

local bending moment m_z and non-linear locally equilibrated, σ_{le}, components (Lidbury 1984) as illustrated in figure 3. As shown in section 6.1 this approach is useful because the local driving force for a crack or flaw can often be expressed simply in terms of the additive effects of these three components.

3. Destructive methods of residual stress measurement

Destructive methods of residual stress measurement rely on the fact that when a cut is introduced the object deforms as the necessary components of tractions due to the residual stress field reduce to zero at the newly formed surface. Common to all these methods is the reconstruction of the original stress field or eigenstrain distribution, from the observed distortion. Central to this is the assumption that the redistribution that takes place as a consequence of cutting does so entirely elastically, introducing no further misfit. Many cutting methods if undertaken carefully (e.g. drilling, water jet cutting, electrodischarge machining and focused ion beam milling) can lead to minimal alteration of the eigenstrain except very local to the cut. However, when near yield stresses are present, removal of constraint may lead to plastic deformation invalidating the technique. The *Standard Test Method for Determining Residual Stresses by the Hole-Drilling* (ASTM E837) specifies that when hole drilling the stresses found should be below 50% of yield. While corrections can be made for this effect for bulk residual stresses up to about 90% of yield (Beghini *et al* 1994), this is rarely done in practice.

3.1. Sectioning

One of the earliest ways proposed for measuring residual stresses involves the complete excavation of blocks upon which strain gauges are attached. It is normally assumed that the block is sufficiently small that the residual stress is completely relaxed. An important question is therefore raised as to the maximum size of block for which stresses having a given characteristic length, l_y, would be essentially relaxed. An answer to this question is obtained by considering a structure with an idealized sinusoidal stress variation (figure 4) and cutting out a block of dimensions y_o, z_o. Clearly the stresses normal to the cut surface must fall to zero at $z = 0$ on making the cut. To estimate the effect this has on the stresses remaining in the
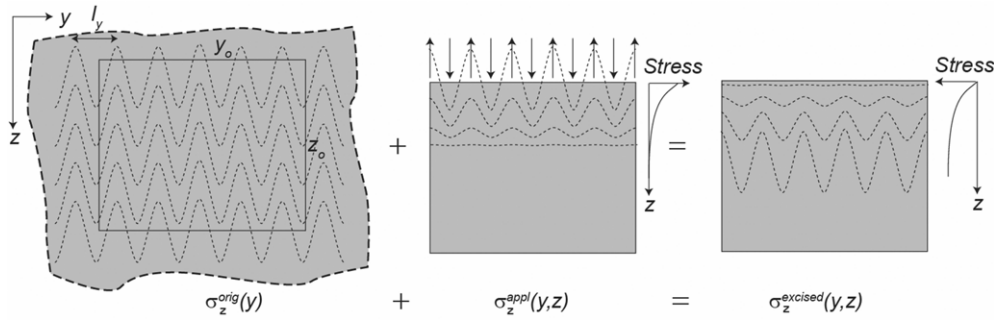
Figure 4. The relaxation of a sinusoidal stress in the z direction having characteristic length, l_y, in the y direction when a block of length z_o is excised, can be estimated by superimposing a sinusoidal variation of opposite sign at the surface of the block.

interior in the block, one should consider the stress field caused by applying a similar sinusoidal variation, but of opposite sign, to the surface of an unstressed block of the same dimensions. This stress will tend to decay to zero towards the interior (figure 4). Superimposing the two stress fields reduces the stress at the surface to zero. With the stresses in the interior given by equation (3a) (Nishioka *et al* 1974, Timoshenko and Goodier 1982).

1D sine fluctuation:

$$\sigma_{zz}(z) = \left[1 - \left(\frac{2\pi}{l_y} z + 1 \right) \exp\left(-\frac{2\pi}{l_y} z \right) \right] A \cos \frac{2\pi x}{l_y}. \tag{3a}$$

2 perpendicular sine fluctuations:

$$\sigma_{zz}(z) = [1 - (kz + 1) \exp(-kz)] A \cos \frac{2\pi x}{l_x} \cos \frac{2\pi y}{l_y} \tag{3b}$$

where

$$k = \sqrt{\left(\frac{2\pi x}{l_x} \right)^2 + \left(\frac{2\pi y}{l_y} \right)^2}.$$

From this it is clear that for a 1D sinusoidal fluctuation the stress has attained 10% of the bulk value by a depth $0.1l_y$ and 80% by $0.5l_y$. As a result, if the block is equal to the $0.2l_y$ or l_y then the centre of the block will be stressed to 10% or 80% of the original stress, respectively. Consequently, provided the block is less than $0.2l_y$ the original stress can be taken to relax completely and the determination of the stress is relatively straightforward. For more complex 2D stress fluctuations the effect of the surface falls off more rapidly towards the interior (equation (3b)), requiring shorter blocks for the stress to be stress free.

For excision from a relatively thin (plane stress) plate provided the stress is completely relaxed, the original principal stresses can be inferred from strains measured using a standard three gauge rectangular rosette (0°, 45° and 90°) from (Schajer 2001):

$$\sigma_{\max}, \sigma_{\min} = -\frac{E}{2} \left(\frac{\varepsilon_3 + \varepsilon_1}{1 - \nu} \mp \frac{\sqrt{(\varepsilon_3 - \varepsilon_1)^2 + (\varepsilon_3 + \varepsilon_1 - 2\varepsilon_2)^2}}{1 + \nu} \right), \tag{4}$$

where $\sigma_{\max}$ and $\sigma_{\min}$ are the maximum and the minimum principal stresses, and ε_1, ε_2 and ε_3 are the readings from the three strain gauges of the rosette. Schajer (2001) differentiates between excision, for which the removed block is small thus becoming stress free, and sectioning, for which only partial strain relaxations occur and for which more sophisticated analyses are necessary.

3.2. Hole drilling

The hole-drilling method involves drilling a shallow hole around which the local surface deformations are measured by a specially designed strain-gauge rosette. Provided the stress is essentially constant over the drill depth the residual stress that originally existed at the hole location can then be calculated from the measured strain relaxations ε_1, ε_2 and ε_3 around it using

$$\sigma_{\max}, \sigma_{\min} = -\frac{E}{2}\left(\frac{\varepsilon_3 + \varepsilon_1}{(1+\nu)\bar{a}} \mp \frac{\sqrt{(\varepsilon_3 - \varepsilon_1)^2 + (\varepsilon_3 + \varepsilon_1 - 2\varepsilon_2)^2}}{\bar{b}}\right), \qquad (5)$$

where $\bar{a}$ and $\bar{b}$ are dimensionless calibration constants depending on the diameter and depth of the hole (Schajer 1988). It is the most mature (Mathar 1934, Rendler and Vigness 1966) and widely employed destructive method.

Depth profiling can be undertaken by drilling incrementally while the strains around the hole are recorded. The sensitivity of the method falls off rapidly with increasing depth. As a consequence the diameter to depth ratio of 1 is a practical limit. Recent bench-marking (Grant and Lord 2002) has been undertaken comparing four techniques for analysing the measured strain data: the uniform stress, equivalent uniform stress (Vishay 1993), power series (Schajer 1981) and Integral methods (Schajer 1988). This has shown that the integral method is most applicable for non-uniform stress fields, in particular those where the stress varies rapidly with depth.

A number of variants in methodology have been developed to extend the hole-drilling method to larger depths. The ring-core method (Milbradt 1951) involves attaching a specially designed strain-gauge rosette. Instead of drilling a hole through the centre of the specially designed rosette, an annular groove is milled around a gauge. This creates an essentially unconstrained island in the material. Because of this full stress relief at the rosette location occurs and equation (5) can be used to infer the stress. Schajer (2001) asserts that in contrast to hole-drilling, the method can be used even when the bulk residual stresses approach the material yield stress because of the lower levels of stress concentration. The deep hole method is a more recent variant (Leggatt *et al* 1996). It is an extension of the geological method developed by (Hooker *et al* 1974) in which a small reference hole is drilled through the thickness to the required depth. Then a larger diameter core is removed concentric with the reference hole. Changes in the diameter of the reference hole as a function of depth can then be related directly to the in-plane stress distribution.

3.3. Slotting methods

The slotting method, also called the crack compliance method (Gruver and Buessem 1971, Vaidyanathan and Finnie 1971, Nowell 1999, Prime and Hill 2002), generally provides a measure of the stress perpendicular to the slot and is applicable when there is little stress variation parallel to the line of the slot. A slot is cut incrementally and the change in gauges located on both the top (close to the crack) and bottom surfaces recorded. The former has more sensitivity when the slot is shallow and the latter more sensitivity when it is deep (Prime 1999). Various procedures exist for reconstructing the original stress profile (Cheng *et al* 1991).

3.4. Contour method

This new technique involves making a planar wire electrodischarge cut completely through a rigidly held specimen (Prime 2000, 2001). Upon cutting, the relaxation of the out-of-plane
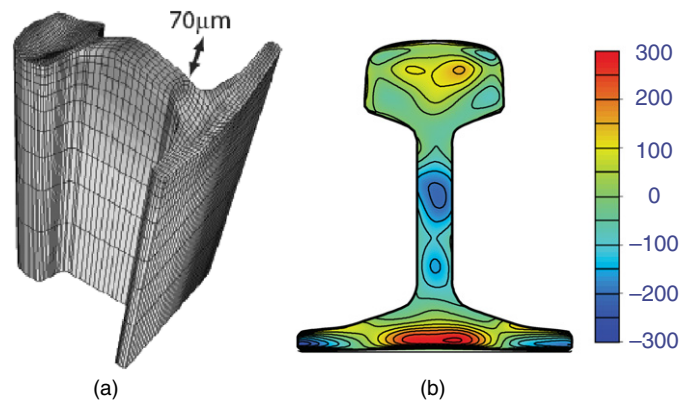
Figure 5. (*a*) Longitudinal displacement (exaggerated, see 70 μm scalebar) measured on the cut surface of a new roller straightened rail (after EDM cutting), (*b*) the component of longitudinal residual stress in the sample (before EDM cutting) inferred by returning the cut surface to flatness (Kelleher *et al* 2003).
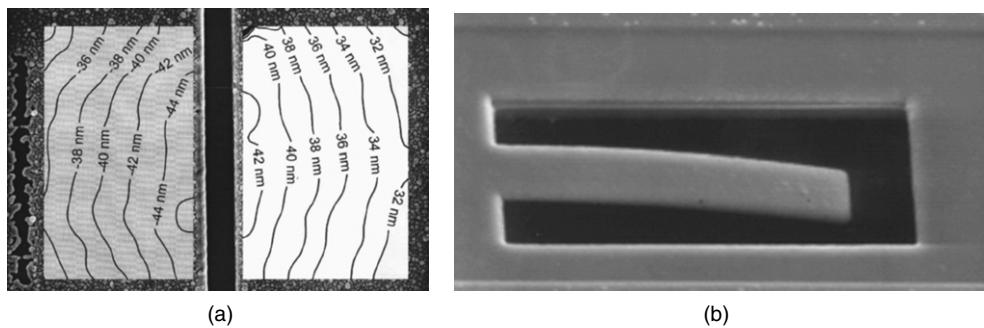
Figure 6. (*a*) Experimentally determined lateral displacement field obtained by image correlation analysis prior, and subsequent, to slitting superimposed on a SEM image of the slit (slit width 300 nm) (Sabate *et al* 2006) in a 300 nm thick Si_3N_4 micromachined membrane and (*b*) 1 μm Al film deposited on a 0.6 μm thick Si micromachined cantilever with deflection recorded by SEM secondary image (McCarthy *et al* 2000). (*a*) Reprinted with permission from Sabate *et al* (2006). Copyright 2006, American Institute of Physics. (*b*) Reprinted with permission from McCarthy *et al* (2000). Copyright 2000 Elsevier.

stress component causes the surface to deviate from planarity (figure 5(*a*)). By measuring the profile of the newly created surface, the original out-of-plane residual stress can then be uniquely calculated using a finite element model in which the distorted surface is forced back into a planar state.

3.5. Microscale stress measurement for microdevices and coatings

Many of the destructive methods described above are now being extended down to the microscale through the availability of dual beam focused ion beam (FIB) micromachining. Using a FIB instrument it is possible to cut, slit, excavate and machine at the nanoscale. For example, slotting has been used to examine the stresses in microelectromechanical systems (MEMS) (Sabate *et al* 2006), as well as in diamond-like films (Kang *et al* 2003). Deformation is deduced from images acquired before and after cutting via the movement of markers or

by image tracking of the surface. Figure 6(*a*) shows the lateral deformation on cutting a through-thickness slot in a 300 nm thick CVD deposited Si_3N_4 membrane. These membranes are used as mechanical supports in a wide range of membrane-based sensors. Such films are typically subjected to ion implantation, to reduce the level of tensile residual stresses. The slotting technique gave residual stresses of 950 ± 40 MPa and 345 ± 10 MPa prior to, and after, ion implantation. Coating stresses have also been estimated from the deflection of thin film cantilevers (figure 6(*b*)) (McCarthy *et al* 2000).

4. Non-destructive methods of stress measurement

Diffraction is perhaps the most important non-destructive means of determining residual stress fields within crystalline materials and engineering components. The principle is simple; the crystalline lattice is used like an atomic strain gauge. Not long after the Braggs had developed Laue's idea that a crystal would act as a diffraction grating to determine crystal structures in 1912, the potential of using the same technique to determine changes in lattice spacing, i.e. to measure elastic strain, was appreciated. The underlying equation is Bragg's equation:

$$\lambda = 2d_{hkl} \sin \theta, \tag{6}$$

which relates the lattice plane spacing d_{hkl} for the (hkl) reflection to the incident wavelength λ and the diffraction angle θ, which is equal to half the scattering angle (2θ). Increases or decreases in the lattice plane spacing are recorded as angular shifts $(\Delta\theta$ in radians) in the diffraction peak positions:

$$\varepsilon_{hkl} = \frac{d_{hkl} - d_{hkl}^{o}}{d_{hkl}^{o}} = -\cot\theta \, \Delta\theta, \tag{7}$$

where d_{hkl}^{o} is the strain-free lattice spacing (often referred to as *d*-zero). Lattice strain is largely insensitive to the plastic component of strain. This is because dislocation generation and motion is the main mechanism of plastic deformation and while the passage of a dislocation through a crystallite causes a permanent shape change once it has passed through, it leaves the lattice spacing unaltered. Of course plasticity does have a second order effect, both due to the constraint of the deformed grain on its neighbours (intergranular type II stress (section 2.2)), and the strain field local to each dislocation contained within it (type III stress). The (elastic) lattice strain can be related directly to stress using appropriate elastic constants. However, since there are many other factors besides stress that can lead to changes in the measured lattice spacing (e.g. local changes in composition, changes in temperature or geometrical effects associated with the sample), great care needs to be exercised during interpretation of lattice spacings in terms of strain (Withers *et al* 2007).

Three main types of radiation are available with wavelengths suitable for measuring atomic lattice spacings, namely, electron, x-ray photon and neutron beams. The three beams can travel very different distances into crystalline materials before attenuation becomes significant (table 1) and so their uses are quite different.

The stiffness tensor, C, allows one to determine the stress tensor from the strain tensor. However conversion from elastic lattice strain to stress is complicated by the fact that, except for tungsten which is isotropic, different lattice planes, *hkl*, have different stiffnesses (e.g. Nye 1985, Tomé 2001). As a result, in a polycrystal under load all the different grain families constrain one another and are thus differently stressed and elastically strained even prior to the onset of plasticity. These integranular stresses and strains depend on the degree of single crystal anisotropy as well as the texture (degree of preferred orientation of the grains). Diffraction by its very nature selects just one grain family, namely, the one having the appropriate *hkl* planes

Table 1. Penetrating properties of different beams characteristic of different sources for steel. The attenuation length (mm) is the path over which the signal will drop to $e^{-1}(=e^{-\mu x})$ where μ is the linear absorption coefficient.

	Energy (keV)	Wavelength (Å)	Attenuation length (mm)
Thermal neutrons (reactor)	2.5×10^{-05}	1.80	8
X-rays (synchrotron)	150	0.08	7
X-rays (synchrotron)	50	0.25	0.7
X-rays (lab. Cu Kα)	8.05	1.54	0.004
Electrons (microscope)	200	0.025	$\sim 1 \times 10^{-4}$

correctly oriented for diffraction. If the single crystal stiffness tensor were used to calculate the stresses from the strains in this particular grain family the stress tensor thus obtained would not correspond to the continuum macrostress, but rather the sum of the macrostress and the intergranular stress. In order to infer the macrostress one uses diffraction elastic constants that relate the strain in a particular grain family, *hkl*, to the continuum macrostress. Generally, the elastic constants are intermediate between those of the single crystal and the bulk response because each polycrystal grain is constrained by its neighbours (Hill 1952). In cases where there is strong texture it is probably best to determine the diffraction elastic constants experimentally using a calibration experiment. In the case of random texture, the bulk polycrystal is elastically isotropic overall and they can be predicted from the single crystal elastic constants (Kröner 1958). For an isotropic solid only two elastic constants are required, E_{hkl} and ν_{hkl} (or the diffraction elastic constants $S_1 = -\nu_{hkl}/E_{hkl}$ and $S_2/2 = (1+\nu_{hkl})/E_{hkl}$):

$$\sigma_{pq} = C_{pqrs}\varepsilon_{rs} = \frac{E_{hkl}}{1+\nu_{hkl}} \left(\varepsilon_{pq} + \frac{\nu_{hkl}}{1-2\nu_{hkl}} \varepsilon_{pp}\delta_{pq} \right), \tag{8}$$

where E_{hkl} and ν_{hkl} are the plane-specific analogues of Young's modulus and Poisson's ratio.

4.1. X-ray diffraction methods

Characteristic x-rays from laboratory sources typically attenuate over path lengths of the order of micrometres to hundreds of micrometres in most engineering alloys (table 1). In fact in back-scattering geometry, the fraction of the total diffracted intensity arising from a surface region of depth z is given by $\{1 - \exp(-2\mu x/\sin\theta)\}$, where μ is the linear absorption coefficient and θ the diffraction angle (Noyan and Cohen 1987), this equates to 95% of the diffracted signal emanating from the top $5.5\,\mu$m for steel using Cu K$_\alpha$ radiation to record the (2 2 2) reflection at $\theta = 69°$. As a result lab. x-ray methods sample the stress state of the very near surface so that x-ray diffraction must be combined with layer removal methods which take into account the effect of material loss to obtain depth profiles (Moore and Evans 1958, Fry 2002). Even with layer removal, depths of only 1–2 mm can be evaluated so that neutron and synchrotron x-ray methods are more suited to deep measurements. The $\sin^2\psi$ x-ray method of stress determination has been used for over 80 years (Lester and Aborn 1925). In essence, measurements are made over a range of inclination angles (ψ) using a high scattering angle (2θ) (figure 7(a)). It exploits the shallow penetration to invoke the bi-axial stress assumption. This leads to the relation (e.g. Cullity 1978, Noyan and Cohen 1987, Hauk 1997):

$$\frac{d_\Psi - d_o}{d_o} = \frac{1+\nu}{E}\sigma_\phi \sin^2\Psi - \frac{\nu}{E}(\sigma_{11} + \sigma_{22}), \tag{9}$$

where σ_{11} and σ_{22} are the principal in-plane stresses and σ_ϕ is the in-plane stress corresponding to $\psi = 90°$. This predicts a linear variation in d_ψ with $\sin^2\psi$ from which the slope can be
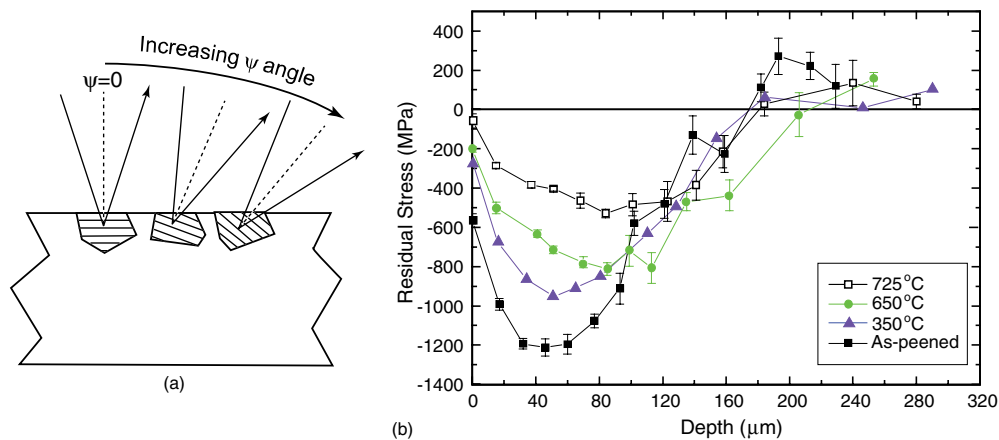
Figure 7. (*a*) Schematic illustrating the $\sin^2 \psi$ technique whereby the in-plane stress can be deduced from the variation in atomic lattice spacing as the ψ angle is increased. Only grains with the relevant lattice plane spacing normal to the dashed line diffract at any given angle, (*b*) residual stress as a function of depth for as-peened Udimet 720Li Ni superalloy and after thermal exposures for 10 h at temperatures between 350 and 725 °C measured by x-ray and layer removal. (Kim *et al* 2005).

used to determine the in-plane stress, σ_ψ. The great advantage of this method is that since the strain-free lattice spacing, which is difficult to determine in practice, is a multiplier to the slope it can be replaced by $d_{\psi=0}$ without significant error (elastic strains are typically significantly less than 1%). A good example of the technique is provided by measurements of the relaxation of shot peening stresses by elevated temperature exposure of Ni superalloy (figure 7(*b*) (Kim *et al* 2005). There are cases where significant gradients in out-of-plane stress can arise over the penetration depth ($l_{\mathrm{II}} <$ penetration depth), for example, in particulate composites and two phase materials (Watts and Withers 1997). Such stress gradients have been shown to introduce curvature into the $\sin^2 \Psi$ plot (Noyan and Cohen 1987).

4.2. Synchrotron x-ray diffraction methods

Third generation synchrotron sources such as the European Synchrotron Radiation Facility (ESRF) and the Advanced Photon Source (APS) provide intense beams of high energy x-rays that are much more penetrating than characteristic lab. x-rays opening up new opportunities for residual strain measurement (Lebrun *et al* 1995, Daymond and Withers 1996, Webster *et al* 1996). As a result synchrotron x-ray beamlines are expanding the envelope of sub-surface residual strain measurements, both in terms of spatial resolution (e.g. 0.5 μm strain measurement grain by grain in electronic structures (MacDowell *et al* 2001)), and the extent and detail that can be mapped. Either single diffraction peaks can be acquired using monochromatic radiation as a function of diffraction angle, or complete diffraction profiles can be acquired at a given angle (figure 8(*a*)) using an energy sensitive detector. Analogous to monochromatic and white beam time-of-flight methods for neutron diffraction, the former typically achieves the best diffraction peak resolution, as well as providing the opportunity to insert an analyser crystal before the diffracted beam reaches the detector. This significantly reduces the sensitivity of the diffraction peak shifts to incomplete gauge filling as occurs when the gauge enters or leaves the sample (Withers 2003). The latter records many diffraction peaks simultaneously and so is well suited to dynamic in situ residual stress studies for example looking shape memory related transitions. It has the added advantage that it is less sensitive to textural changes and
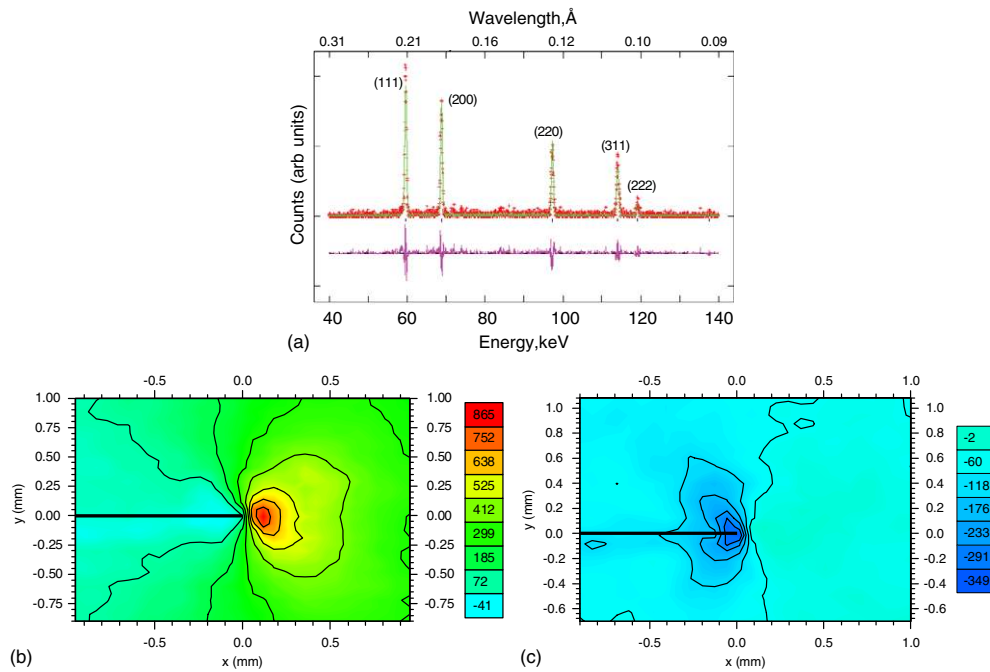
Figure 8. (*a*) Typical spectrum collected on beamline ID15A at the ESRF in energy-dispersive mode at $2\theta = 5°$ for the specimen studied in (*b*, *c*), (*b*) elastic crack opening (*y* direction) stresses (in MPa) mapped using a 25 μm beam in a 12 mm thick Al–Li compact tension fatigue cracked test specimen 100% over-loaded to a stress intensity of $2K_{max} = 13.2$ MPa m$^{1/2}$ and (*c*) the residual stresses after unloading to $K_{min} = 0.6$ MPa m$^{1/2}$ caused by the overload event. The crack is approximately located at (0,0) (Steuwer *et al* 2007).

all the diffraction peak positions can be refined simultaneously to provide a measure of the bulk elastic strain for which the elastic constants representative of the bulk can be used to infer stress. Typically the diffraction angles are small due to the short wavelengths associated with the high energies needed for bulk studies.

Figures 8(*b*) and (*c*) exemplify what can be achieved showing how a 100% overload event during fatigue cycling introduces residual stresses in the vicinity of the fatigue crack at the mid-plane of a 12 mm thick Al–Li alloy compact tension sample at a lateral spatial resolution (25 μm). Note that the crack is located at approximately $x = 0$ mm indicating compressive residual strains in figure 8(*c*), both across the crack flanks ($x < 0$ mm) and just ahead of the crack ($x > 0$ mm). This is also shown in the linescans shown in figure 31. Grain size restraints mean that this lies close to the spatial limit of what can be achieved using powder diffraction methods to study crack-tip stress fields deep within materials (Steuwer *et al* 2007).

4.3. Neutron diffraction methods

Thermal neutron beams are very penetrating (table 1) on account of the fact that the particles are chargeless. Their potential for residual strain measurement has been recognized since the early 1980s (Allen *et al* 1981, Pintschovius *et al* 1981). Because neutron fluxes are typically orders of magnitude less than synchrotron x-ray photon fluxes; experiments are best suited to acquiring line profiles or limited 2D scans using millimetre sized gauge volumes, rather than detailed 2D/3D maps at sub-millimetre resolution. Single peak measurements can be made
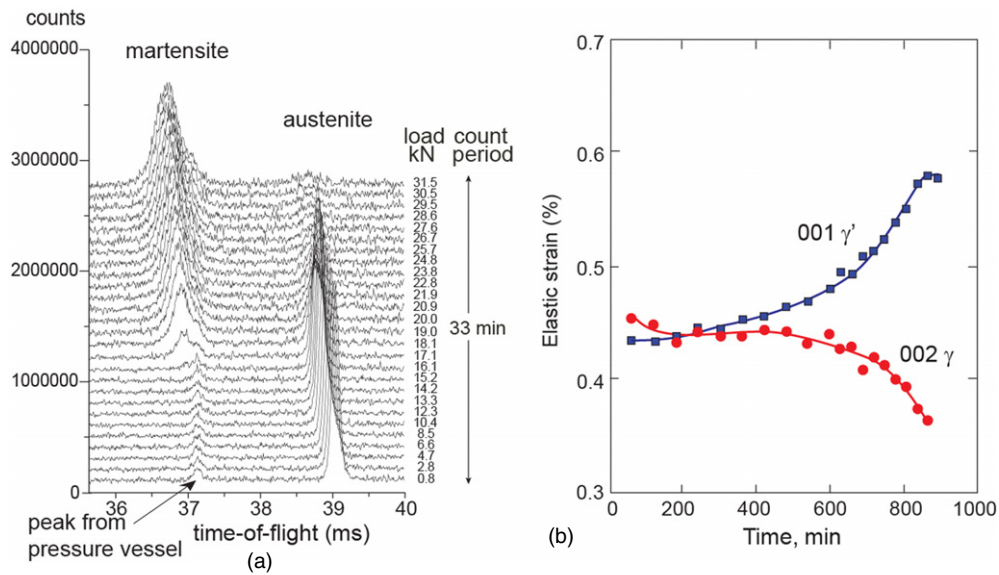
Figure 9. (*a*) Stacked neutron diffraction patterns over part of the time-of-flight range collected for superelastic NiTi samples deformed at 160 MPa confining pressure. The changing relative proportion of the austenite and martensite phase is apparent in the changing peak intensities, while the increasing elastic strain in each phase is visible as a shift in peak position (Covey-Crump *et al* 2006) and (*b*) the repartitioning of phase specific strains in oriented γ and γ' grains in polycrystalline Ni-base superalloy, CM247 LC having 65% volume fraction of the γ' phase, during the tertiary stage of creep at 425 MPa and 900 °C (Ma *et al* 2005).

using a monochromatic beam (suited to reactor sources), or multiple peak profiles acquired simultaneously at set angles in 'time-of-flight' mode, typically at pulsed spallation neutron sources (Hutchings *et al* 2005). In the latter case the wavelength of each detected neutron is inferred from its time-of-flight, t, and the path length, L_n, from moderator to detector;

$$\lambda = ht/m_n L_n, \tag{10}$$

where m_n is the mass of the neutron and h Planck's constant. Because thermal neutrons are highly penetrating, samples can be studied in situ under complex environmental conditions which are inaccessible or too hostile for other methods. For example much work has been done under hydrostatic pressures, elevated temperatures and loading cycles (see figure 9).

4.4. Other methods

There are many other means of evaluating the residual stress. These rely on the fact that some other property is related to the stress, e.g. Raman excitation or photoluminescence (Mollis and Clarke 1990, Young 2001), magnetic response in magnetoelasticity (Hyde *et al* 2000, Buttle and Scruby 2001, Han *et al* 2002) (e.g. Barkhausen noise, magnetic permeability, etc) or electrical properties (Schoenig *et al* 1995, Blaszkiewicz *et al* 1996, Blodgett and Nagy 2004), speed of sound in acoustoelasticity (Pao *et al* 1984, Guz and Makhort 2000), optical properties in photoelasticity (Patterson 2001) and temperature change due to adiabatic heating in thermoelasticity (Wong 2001, Quinn *et al* 2004). On the plus side many of these are non-destructive, portable and relatively cheap to apply. However, in most of these cases it is
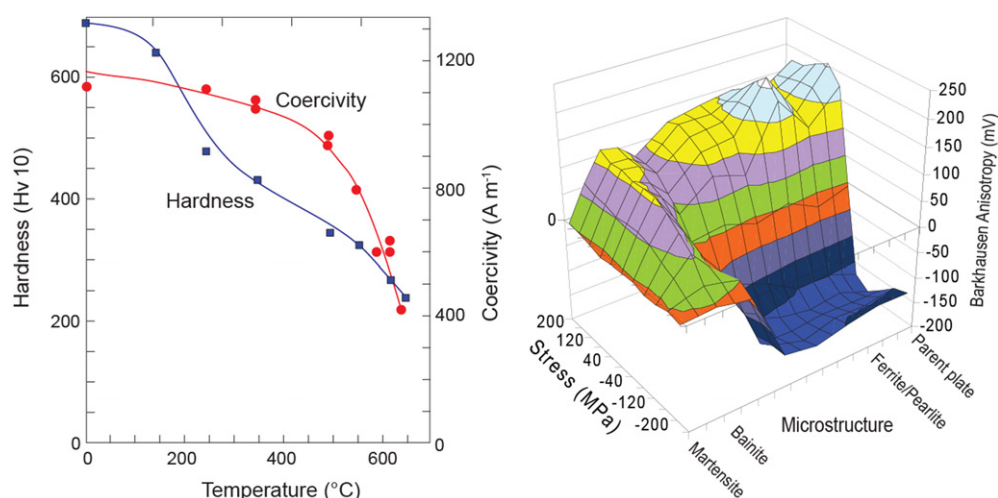
Figure 10. (*a*) Hardness and coercivity for 4360 steel following homogenization at 1000 °C, water quenching and tempering (Buttle *et al* 1987). (*b*) In-plane anisotropy of Barkhausen emission measurements made as a function of applied uniaxial stress for steel subjected to various peak temperatures and cooling rates in order to simulate heat affected zone microstructures (Buttle and Scruby 2001). Note how the martensitic phase is largely insensitive to stress.

difficult to derive their quantitative relationship to stress from first principles; instead these methods tend to rely on calibration experiments to extract the relationship between measured variables and stress (e.g. magnetics, Raman) and to account for microstructural and chemical dependencies.

By way of an example consider the magnetic response. The interaction between the atomic moments in the lattice causes their alignment into magnetic domains (ferromagnetism), which in turn generates a small strain in the lattice (magnetostriction). This coupling between strain and domain orientation means that under stress, it becomes energetically favourable for the orientation distribution of magnetic domains to change, so that in steel (positive magnetostriction), the magnetization vector points towards the tensile axis thereby reducing the magnetoelastic energy. However, this redistribution of domains tends to increase magnetostatic energy so that a balance between these terms is achieved. The changes in magnetic domain distribution mean that magnetic hysteresis, permeability and remanence are all functions of the stress tensor. Critically other factors such as texture, phase transformations, the presence of alloying elements, plastic strain and geometrical effects can also affect the response necessitating careful interpretation and meaning that it is not possible to quantify the relationship between primary magnetic parameters and stress without experimentation. A good example is provided by the magnetic behaviour of 4360 (0.5% C) steel as a function of tempering following water quenching from 1000 °C (Buttle *et al* 1987). As quenched, the largely martensitic structure exhibits a high coercivity (figure 10(*a*)). With increasing growth of ferrite and precipitation of cementite the coercivity falls significantly. An added complication in the magnetic case is that it is not generally possible to measure primary magnetic parameters (coercivity, remanence, etc) at a point within a component and thereby evaluate stress. Rather, less direct measures of the magnetic response, such as *Barkhausen noise (BN), stress induced magnetic anisotropy* and *directional effective permability* are recorded (Buttle and Scruby, 2001). These are instrument specific and this is hampering the development of an unambiguous, universally agreed approach to magnetic stress measurement. BN comprises essentially

electromagnetic pulses arising from irreversible domain wall movements under an applied magnetic field (Tiitto 1977, Buttle *et al* 1987). It depends upon the domain distribution and hence the stress state. The domain wall pinning sites can be dislocations, second phases or grain boundaries. Consequently this technique is particularly sensitive to the microstructure and mechanical properties of the material (Buttle and Scruby 2001) (figure 10(*b*)). Because of the difficulties associated with unequivocal interpretation of the signals in terms of particular stress components, many of these methods are best suited to specific applications, where the likely microstructural effects have been well characterized.

5. Origins of residual stress

5.1. Plastic deformation

In a real material plastic deformation is never completely homogenous. Deformation at the atomic scale takes place by the movement of discrete line defects (dislocations) through the crystallite. Of course there are many other reasons why deformation may be inhomogeneous, for example at the intergranular level due to differences in slip behaviour between differently oriented grains, termed plastic anisotropy (Clausen *et al* 1999, Pang *et al* 1999), or the difference between different phases (Noyan and Cohen 1985, Withers and Clarke 1998), or at the macroscale due to local differences in the yield stress, the existence of stress concentrators (e.g. holes, geometrical features, etc), or to the external application of non-uniform loads. Probably the simplest way to introduce a residual stress plastically into a body such as a bar is to bend it beyond the elastic limit. This was one of the first residual stress distributions to be evaluated by neutron diffraction (Pintschovius and Jung 1983) (see figure 11). For geometrical reasons the total strain across the bar must vary linearly as represented by the dashed line. Within the elastic region the lattice strain and strain gauge response agree. Once the yield stress is exceeded on the outer surfaces the plastic zones expand inwards; such that the elastic strain represented by the lattice strain and the plastic strain equal the total strain. The resulting plastic strain misfit between the outer regions and the elastically strained interior is maintained on elastic unloading such that the bar remains permanently bent, as recorded by the strain gauge and a characteristic zig-zag residual strain profile results. The compressively strained (LHS) region has tensile residual strains while the tensilely strain region (RHS) is compressively strained.

5.2. Thermal origins

Thermal misfit stresses arise due to temperature gradients within a body. Consider for example, rapid cooling (quenching); the exterior which cools fastest would contract naturally due to the decrease in temperature were it not for the resistance offered by the warmer interior. This generates tensile stresses in the exterior and compressive stresses in the interior. Normally, these stresses are transient disappearing when the body as a whole reaches the same temperature. If on the other hand the gradients are sufficiently severe (thereby generating significant stresses), or the yield stress of the interior very low (due to the elevated temperature), then non-uniform plastic deformation may occur in regions where the yield stress is exceeded. Once cooled to a uniform temperature these permanent misfits generate a characteristic residual stress. This method is used commercially to introduce compressive in-plane surface stresses in thermally toughened glass. The sequence of stress profiles as the glass is cooled rapidly from above the glass transition temperature is shown in figure 12(*a*). Once cooled these residual stresses are not evident from the appearance of the glass, but radically affect the
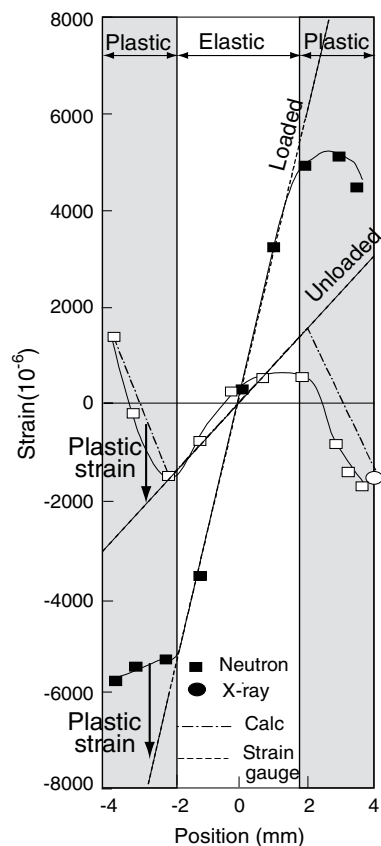
Figure 11. Lattice strain variation across an aluminium alloy bar loaded with a bending moment (163 Nm) exceeding the yield point of the material: filled symbols denote measurements under load, open symbols measurements after the load had been released; the dashed line denotes the engineering strain under load and the dashed–dotted line the residual strain predicted on the basis of elastic–plastic bending (Pintschovius and Jung 1983).

failure behaviour of the glass leading to a characteristic mosaic crack that runs through the interior of the glass pane. Because it is the elastic strain energy that provides the energy to produce such a network of cracks, the residual stress can be estimated from the average size of the pieces (Bilby 1980). Using a typical value for the fracture energy $R \approx 10\,\text{J}\,\text{m}^{-2}$, and the residual mid-plane tensile stress $\sigma^T \approx 50\,\text{MPa}$ (figure 12(a)), then the stored elastic energy per square metre, $\sim (1 - \nu)(\sigma^{T^2}/E)d$, of a plate of thickness d is equal to the work $(4R/x)d$ needed to shatter it into pieces of size x. This simple analysis gives t $\sigma^{T^2}x$ a constant, or equivalently fragment mass $\sim x^2 \sim 1/\sigma^{T^4}$ as shown in figure 12(b), with a typical fragment size around 10 mm. Similar stresses are introduced in age-hardenable Al alloys as a necessary consequence of the quenching stage used as part of the precipitation hardening sequence. These stresses can cause distortion when the billet is machined to final shape. This represents a serious problem in the aerospace industry.

Thermal misfit stresses are generated at a finer scale (type II level) whenever a two phase material is heated or cooled (figure 2) no matter how evenly it is cooled. This is also true for single phase non-cubic crystal structure materials because thermal expansion is anisotropic at the single crystal level (Nye 1985). These stresses can combine with preferred grain orientations introduced by deformation processing to give rise to severe thermal cycling
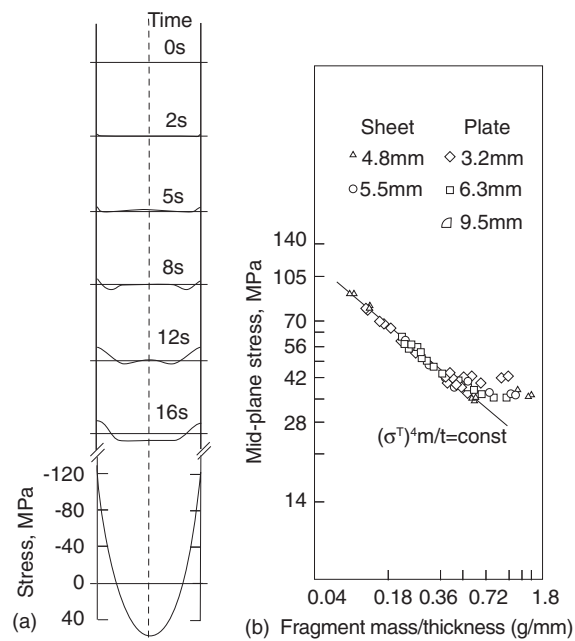
Figure 12. (*a*) Temporal evolution of thermal stresses across a 6.1 mm plate plate during quenching from 738°C (Narayana and Gardon 1969), (*b*) correlation between mid-plane tensile stress and fragment mass in thermally quenched glass (Barsom 1968).

Figure 13. The effect of 850 thermal cycles between 50 and 600 °C on α-uranium bars 25 mm in diameter, originally smooth and of equal length. The different extent of their distortion is due to differences in preferred polycrystal orientation arising from their original mode of fabrication (from left to right, as-cast, hot rolled, cold swaged) (Pugh 1958).

distortion effects in uranium (figure 13). Similarly hexagonal lithium aluminium silicate has expansion coefficients of $+6.5 \times 10^{-6}$ and -2.0×10^{-6} K^{-1} across and perpendicular to the basal plane, meaning that as a polycrystal it has a very low thermal expansion coefficient overall making it a good choice for ceramic hobs as used on domestic cookers (Newey and Weaver 1990). By engineering a fine grain size it is possible to minimize the scale of the intergranular thermal stresses and limit the size of intrinsic flaws which tend to scale as the grain size from which failure might initiate.

5.3. Phase transformation

Newnham states (Newnham 1998); '*One of the qualities that distinguishes living systems from inanimate matter is the ability to adapt to changes in the environment. Smart materials have the ability to perform both sensing and actuating functions and are, therefore, capable of imitating this rudimentary aspect of life.*' Many 'smart' materials rely on solid state transformations that occur displacively. Displacive transformations are characterized by a rapid distortion of the crystal lattice from one structure to another, thereby generating a misfit between the transformed and untransformed regions which may give rise to residual stresses (Mori and Withers 2001) as well as a sudden macroscopic shape change. The most well known example of a displacive transformation is provided by the martensitic transformation in steel. In order to minimize the residual stress (elastic energy) the martensite nucleates as lenticular plates with a twinned structure.

Currently, there is much interest in the potential of 'smart' materials that switch or transform under:

- deformation, including TRIP steels (Cherkaoui *et al* 1998, Oliver *et al* 2002, Zrnik *et al* 2005), superelastic (Vaidyanathan *et al* 1999) and shape memory materials (figure 14) (Dunand *et al* 1996, Berveiller *et al* 2004, Hornbogen 2004, Kaouache *et al* 2004, Oliver *et al* 2005),
- temperature (thermally activated shape memory materials) (figure 15(*a*)) (Liu *et al* 2005, Karaca *et al* 2003),
- electric fields (ferroelectrics, piezoelectrics (figures 15(*b*) and (*c*)) (Huber and Fleck 2001, Hall *et al* 2005, Li *et al* 2005)) and
- magnetic fields (Inoue *et al* 2002).

Potential applications include (Van Humbeeck 1999); robust spectacle frames, mobile phone antennae, ear phones (these all exploit the superelastic effect), heat-recoverable couplings, heat-to-shrink fasteners, dematable connectors (based on the thermal shape memory effect (see figure 15(*a*))), medical devices such as stents and thermally, electrically and magnetically activated domain switching in actuators and dampers.

Diffraction is well suited to the monitoring of such transformations and for assessing their related residual stresses. This is because the phase selectivity of diffraction allows the tracking of both the extent of the transformation, through the integrated intensity of the transforming phase reflections, and the associated residual stress levels through the peak shifts (figure 9(*a*)). Synchrotron and neutron diffraction have the advantage that the transformation can be studied in the bulk, where the constraint is largest. This is well illustrated by the work of Vaidyananthan *et al* (1999) on superelastic Ni–Ti (figure 14), and Hall *et al* (2005) on lead zirconate titanate (PZT) (figure 15). In the former, The austenite is randomly oriented in the unloaded condition and remains so at least till superelastic straining begins. Upon further increasing the load, the remaining austenite exhibits increasing texture as martensite is formed because of its preferential transformation (figure 14(*c*)). In the ferroelectric example, the reorientation of the spontaneous polarization, through an angle of either 71° or 109°, results in an increase in the fraction of ferroelectric domains oriented along the electric field direction ($\psi = 0°$). Consequently, the relative intensity of the (1 1 1) diffraction peak increased relative to that of the ($\bar{1}$ 1 1) peak in the XRD patterns recorded at $\psi = 0°$ (figure 15(*c*)). The opposite effect is observed in the patterns obtained at $\psi = 90°$. The domain switching process is almost complete for the {1 1 1} grain family at a field of 2.5 MV m^{-1}. On the microscopic level, the poling strain of a grain, $\bar{\varepsilon}^P$, caused by ferroelectric domain switching, depends on its orientation, ψ, relative to the direction of the applied electric field. Each grain experiences a
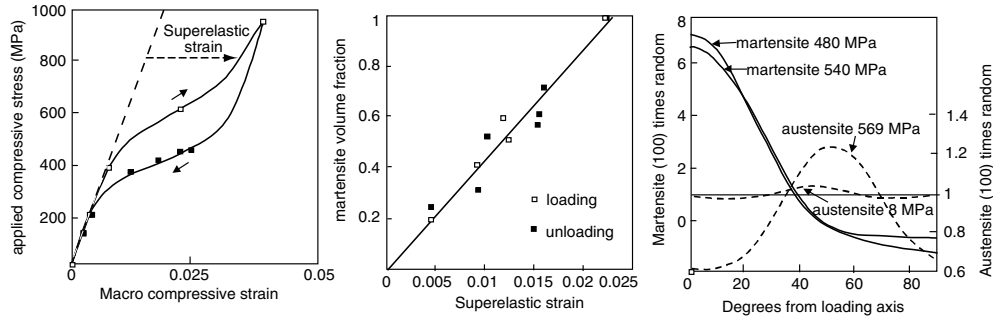
Figure 14. (*a*) Superelastic deformation in Ni–Ti, (*b*) extent of austenite to martensite transformation as a function of superelastic strain and (*c*) (1 0 0) martensite (——) and austenite (- - - -) diffraction peak intensity distributions with increased loading as determined by neutron diffraction (Vaidyanathan *et al* 1999).

misfit strain, $\bar{\varepsilon}^*$, and hence residual stress given by the difference between its individual poling strain, $\bar{\varepsilon}^P$, and the macroscopic strain of the polycrystal, $\langle\varepsilon\rangle$.

$$\bar{\varepsilon}^* = \bar{\varepsilon}^P - \langle\varepsilon\rangle. \tag{11}$$

These results show that the strain of a grain along $\langle 2\,0\,0\rangle$, which would be unaffected by changes in its ferroelectric domain population in a 'free' (unconstrained) state, develops a large tensile component along the macroscopic polar axis on poling (figure 15(*d*)). This elastic strain along $\langle 2\,0\,0\rangle$ is directly related to the preferred orientation caused by ferroelectric domain switching in the surrounding grains, which on average become elongated.

5.4. Welding and other localized heat treatments

In section 5.2 it was pointed out that whenever a material is exposed to severe thermal gradients there is an opportunity for non-uniform plastic deformation: this situation is characteristic of welding. The local thermal excursion usually causes plastic strain in the weld metal and base-metal regions near the weld (figure 16) (Masubuchi 2003). These give rise to residual stresses as well as to local shrinkage and distortion. It should also be borne in mind that the materials microstructure is likely to be sub-optimal locally in that the parent microstructure has usually been optimized to peak condition by careful processing, while the extreme local thermal excursion is likely to have led to a less favourable microstructure from a performance point of view (e.g. softer or less tough). Given this and the fact that joints are often sites of stress concentration these residual stresses are commonly a cause of cracking and premature failure of welded structures. Typically, the residual stress in the weld is largest along the length of the weld in the weld metal and heat affected zone, often being limited by the yield stress as the weld metal cools (figure 16).

Given the very large number of variables involved in welding (torch properties, liquid metal behaviour, solidification, material softening, thermal contact to jig, jigging constraint, etc) it is not currently possible to predict the stresses caused by welding *a priori* (Zacharia *et al* 1995). Instead the process physics is usually simplified (e.g. neglecting the behaviour of the melt, simplifying the heat input, etc). Consequently thermocouple measurements are normally used to determine parameters such as torch efficiency and the efficacy of heat transfer from the welded joint. In addition post-mortem measurements of the fusion zone have been used to help determine certain welding parameters (Kumar and DebRoy 2004).
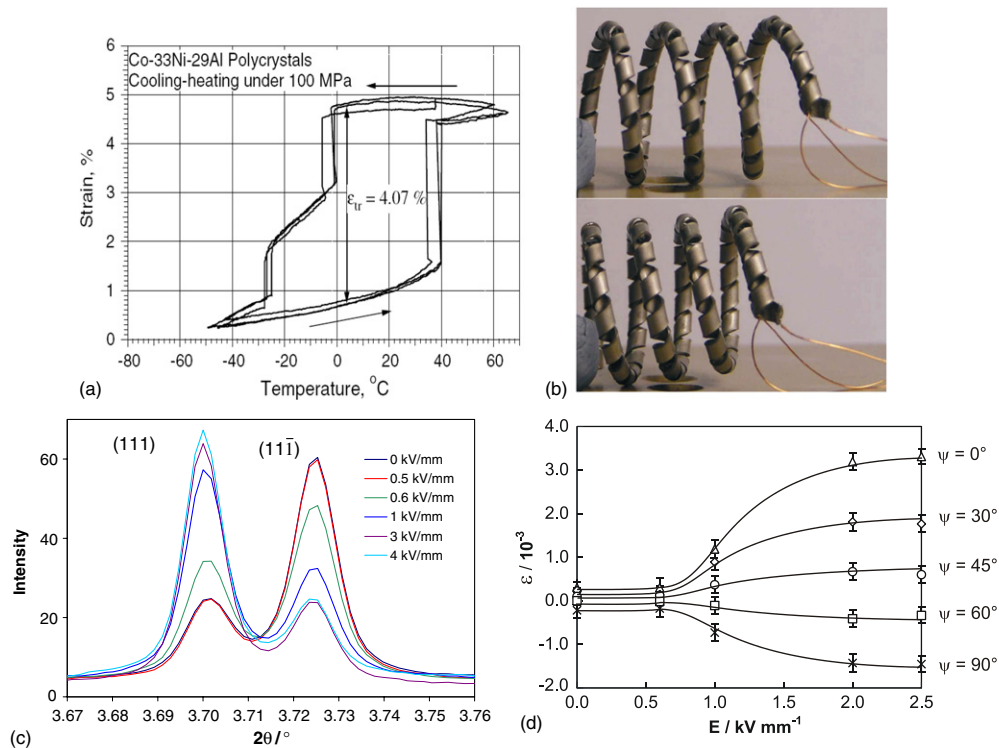
Figure 15. (*a*) Compressive strain versus temperature response for Co–33Ni–29Al under 100 MPa (Karaca *et al* 2003). (*b*) Macroscopic dimension change caused by domain switching during poling of a PZT actuator (courtesy of Hall), (*c*) synchrotron x-ray diffraction shows that domain switching under an increasing electric field for a rhombohedral PZT ceramic increases the (1 1 1) and decreases the (1 1 $\bar{1}$) intensity parallel to the electric field and (*d*) concomitant lattice strain $\varepsilon\{2\,0\,0\}$ as a function of angle to the poling direction due to the macroscopic shape changes.

While most welding methods involve the creation of molten metal (e.g. manual metal arc, tungsten inert gas (TIG) (figure 17(*a*)), etc), it is not necessary for melting of metal to occur for a joint to be formed. Provided the oxide layer can be removed, non-directional metallic bonds can form across the joint without melting. There is an increasing number of solid state joining mechanisms based around generating heat and removing the oxide layer by friction (Nicholas and Thomas 1998). Despite the fact that no melting is involved and thus the local heat input is lower than for conventional fusion welding methods, they are also characterized by significant residual stresses. Joints can be formed by friction stir welding (Thomas *et al* 1991), in which a tool comprising a pin and head is rotated and plunged into the region to be joined much like a drill and moved along the join line. Here plasticized metal is extruded past the tool forming a joint behind it. Inertia and direct drive rotational welding are used to form axially symmetric parts, such as shafts and turbine disc assemblies for aeroengines (Preuss *et al* 2002). Linear friction welding on the other hand relies on a backwards and forward motion to generate the heat (Wanjara and Jahazi 2005). It is well suited to joining blades to aeroengine discs. In common with the fusion welding processes, it is usually the heat distribution and the associated high temperature mechanical properties that play the most significant roles in determining the final residual stresses rather than the plastic deformation (Staron *et al* 2002, Peel *et al* 2003, Reynolds *et al* 2003) as demonstrated by the similarity between the stress fields for friction and fusion welds in figure 17. In fact in many cases the residual stresses and
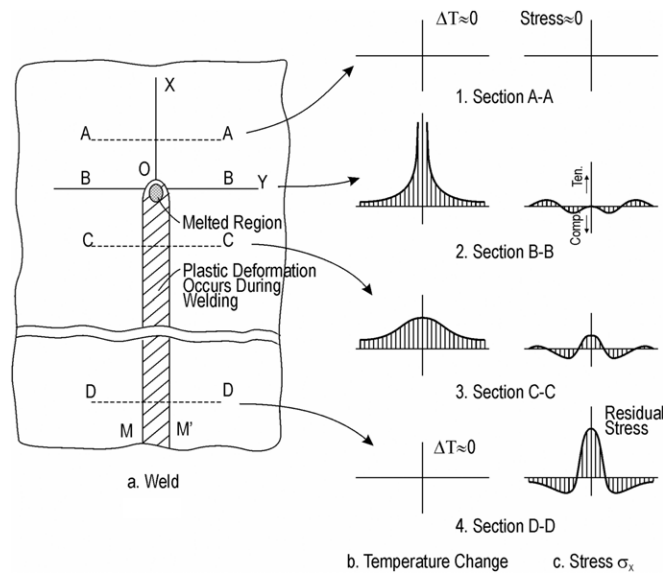
Figure 16. Schematic representation of changes of (*b*) temperature and (*c*) longitudinal thermal residual stresses during bead-on-plate welding (Masubuchi 2003).

microstructure can be well predicted using thermal models that neglect the plastic deformation completely, but consider the heat thus generated in much the same way as a torch inputs heat into a traditional welding process (Richards *et al* 2006, Steuwer *et al* 2006). A review of weld modelling issues is provided by Zacharia *et al* (1995).

5.5. Composites and multiphase materials

Composites are inherently heterogeneous and so there are many opportunities for misfits to arise (Withers *et al* 1989). Amongst others, these may be due to differences in the elastic behaviour (Allen *et al* 1992), plastic deformation (Cheskis and Heckel 1968, Wilson and Konnan 1964) and coefficient of thermal expansion (see figure 2) (Withers *et al* 1987, Saigal *et al* 1992). In many aspects of mechanical performance, it is the heterogeneity in the stress between the phases that is critical in characterizing composite behaviour. As discussed in section 2.2 great care must be taken when selecting an appropriate method to measure the residual stresses since they arise at all length scales. If the gauge volume is small then the stress in an individual fibre (type II stresses) may be measured, for example using micrometre resolution Raman analysis (Huang and Young 1994) or synchrotron diffraction (Sinclair *et al* 2005). If the gauge is large (~mm), but sensitive only to a single phase, such as the case for neutron diffraction, the average mean phase stress is measured (Allen *et al* 1992), while destructive methods tend to measure the phase independent macrostress (Cowley and Beaumont 1997, Retraint and Lu 2000) an exception to this being the finescale cutting of a 200 μm tungsten fibre Kanthal matrix system described in (Prime and Hill 2004).

6. Stress engineering, mitigation and stress relief

Residual stresses are often regarded as unwanted and detrimental. However, as reviewed by Hurrell *et al* (Hurrell *et al* 2006) in respect of power plant, there are many ways either to reduce potentially harmful residual stresses, or to introduce beneficial residual stresses to prolong life.
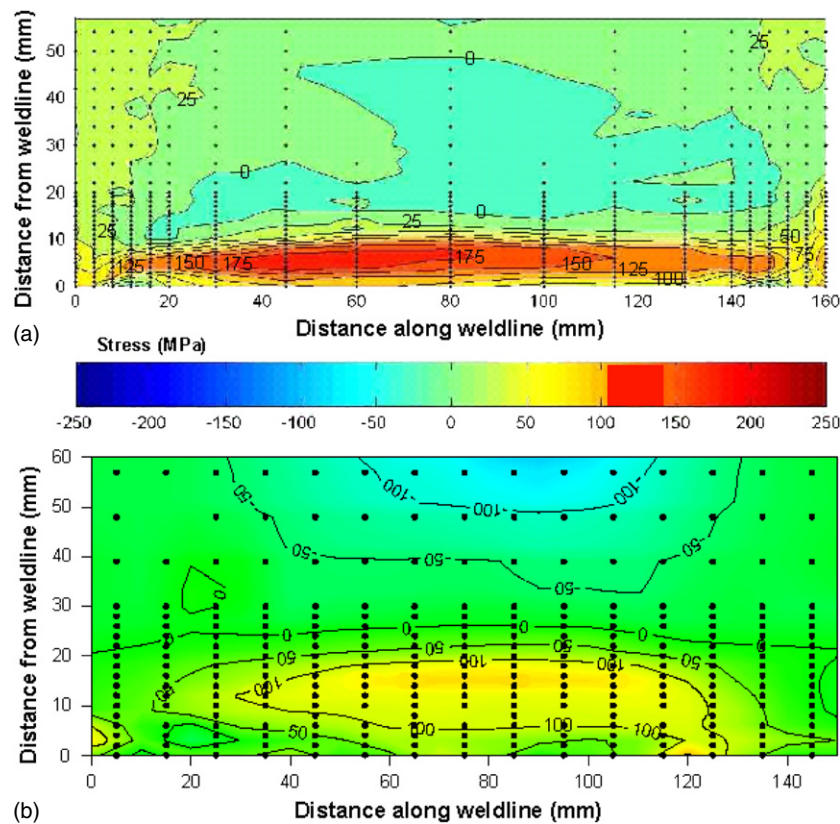
Figure 17. Comparison of the through-thickness longitudinal stresses measured by synchrotron diffraction in (*a*) 3 mm thick conventional Al 2024 TIG fusion welded plate (Withers and Webster 2001), and (*b*) the AA6082 side of a 3 mm thick Al 5083/Al 6082 friction stir welded joint using a tool with a 6 mm pin and 18 mm diameter shoulder rotating at 840 rpm and travelling at 100 mm min^{-1} (Steuwer *et al* 2006). Being a dissimilar weld the stresses on the non-age-hardenable 5083 side of the weld are somewhat different in magnitude. In both welds the weld started around $x = 10$ mm.

6.1. Annealing/post-weld heat treatment

Residual stresses are commonly relaxed by stress relief annealing. Indeed, post-weld heat treatments (PWHT) are routinely applied to welds in safety critical plant. Ideally the whole body is uniformly exposed using slow heat-up/cool-down rates that are slow (1 °C h/25 mm thickness in steel (Hurrell *et al* 2006)). At least two stress relief mechanisms are important; plasticity caused by the reduced yield stress at elevated temperature which occurs essentially instantaneously as the temperature increases, and creep mechanisms which occur over a longer period of time. It should be noted that because plastic strain is deviatoric in nature, the hydrostatic component of the misfit cannot be relieved by local plastic flow but requires larger scale rearrangement. Usually the aim is to relieve stress without significantly altering the underlying microstructure. If the temperature is too high then recrystallization might occur changing properties such as the yield stress which may not be desirable. For a given situation, precise estimation of the rate and nature of the three dimensional relaxation of misfit and thereby residual stress requires numerical modelling as well as a detailed appreciation of the available mechanisms. At an engineering level, it is useful to have simple relations
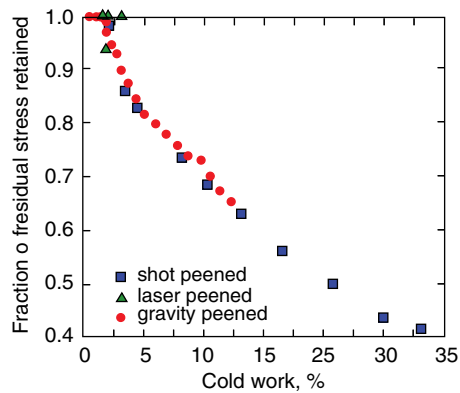
Figure 18. Correlation of cold work and fraction of near surface residual stress retained in shot peened, laser peened and gravity peened IN718 after 10 min at 670 °C (Prevey 2000).

for identifying suitable post-weld heat treatments for relaxing, perhaps, unknown levels of residual stress. Holzapfel *et al* (1998) took a simple empirical approach based on the Avrami relation to obtain an approximate measure of the extent of stress relaxation at a peened surface. Taking stress relaxation to be caused by thermally activated processes, it can be approximated by

$$\frac{\sigma^{\text{rs}}(T, t)}{\sigma_{\text{o}}^{\text{rs}}} = \exp\left(-\left[C \exp\left(-\frac{\Delta H}{kT}\right) t\right]^{m}\right) \tag{12}$$

with $\sigma^{\text{rs}}(T, t)$ the residual stress value after annealing at temperature T (in K) for the time t (min), $\sigma_{\text{o}}^{\text{rs}}$ the initial near surface residual stress, ΔH the activation enthalpy for the actual residual stress relaxation process (=3.3 eV for AISI 4140 stainless steel), m (=0.122) an exponent, C (=1.22 × 10^{21} min^{-1}) a rate constant and k the Boltzmann constant. This relation may have wider utility in estimating the rate of relief of a local maximum stress. For stainless steel this relation gives a 50% reduction after 5 h at 750 K or 8 min at 800 K (note $T_{\text{m}} = 1750$ K). For some specific materials and conditions, for example certain steels used in pressure vessel design specified PWHT guidelines exist, e.g. (ASME 2004). In certain cases it is not practical to treat the whole component. Local PWHT is not as effective as global treatment; care must be taken to ensure a sufficiently large region is heated. For a weld or weld repair to a tube the heating band surrounding the weld is recommended to be greater than $2.5\sqrt{(Rt)}$ where R and t are the tube diameter and thickness, respectively (Hurrell *et al* 2006). There is some evidence that in situations such as peening where there may be significant levels of cold work, that the stored energy may affect the thermal stability of the residual stresses (figure 18). This needs to be borne in mind if relations such as equation (12) are being used to assess the longevity of beneficial residual stresses, and highlights the wisdom of validating PWHT procedures with actual measurements to assure their effectiveness.

6.2. Stress introduction strategies

One of the most effective means of prolonging the fatigue life of a component is by placing the surface in residual in-plane compression (figure 19(*a*)). Most commonly this is achieved by the introduction of plasticity local to the surface region. Traditionally this has been achieved by shot peening, whereby the surface is repeatedly impacted by hard millimetre sized 'shot'. Each impact introduces local plasticity and the net effect is a compressive residual in-plane stress
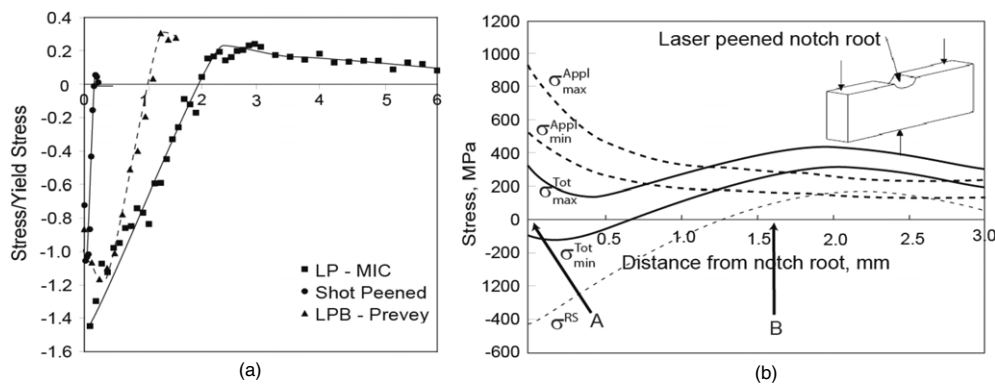
Figure 19. (*a*) Graph showing the different depths characteristic of the different peening methods (LP and shot peening courtesy of Metal Improvement Company), (*b*) residual stress from laser peening, applied stress range (dashed) and total stress (continuous) range for 3 point bending fatigue having an amplitude of ±180 MPa about a mean stress of 730 MPa at the notch root in Ti–6Al–4V (McElhone and Rugg 2005).

to a depth of around 200 μm (see figures 7 and 19(*a*)). This is often sufficient to overwrite potentially harmful near surface stresses, as might be introduced by machining, with beneficial compressive ones prior to service. Fretting (the rubbing of one surface against another) on the other hand can cause these beneficial stresses to decay rapidly in-service by introducing contact induced plasticity to a depth similar to the shot peening depth (King *et al* 2006). Processes such as laser peening which introduce deeper residual stress misfits than are normally relaxed by fretting can confer greater fatigue resistance.

A number of methods have been developed to introduce compressive stresses to greater depths, most importantly laser peening and low plasticity burnishing or deep rolling. Laser peening was developed in the early 1970s (Fairand *et al* 1972); however, it was only when improved laser technology arrived in the 1990s that the method really became feasible. Laser peening involves the illumination of a black sacrificial tape or coating with a short, intense pulse (10–100 ns) of laser light having an energy of up to 25 J over an area as large as 3 mm square (Rankin *et al* 2003). The pulse sets up a plasma which if constrained by an overlay of water drives a shock wave into the substrate. This pressure wave ($\sim$3 GPa pulse with 20 ns duration (pulse energy $\sim$50 J cm^{-2}) (Rankin *et al* 2003)) is sufficient to plastically deform the sample introducing residual stresses to a depth of 1 or 2 mm with no appreciable surface heating (figure 19(*a*)).

Low plasticity burnishing (Prevey and Cammett 2004) is usually performed using a single pass of a free rolling ball under a normal force sufficient to plastically deform the surface of the material. Contact loading creates a layer of compressive residual stress to a depth exceeding 1 mm (figure 19(*a*)). The ball is supported by a fluid bearing with sufficient pressure to lift the ball off the surface of the retaining spherical socket. The ball is free to roll on the surface of the work-piece as the tool progresses.

As illustrated in figure 19(*b*), laser peening can significantly lower the tensile stress experienced at stress concentrators (in this example by about 600 MPa), thereby significantly extending fatigue life. In this case for a high applied notch root mean stress (730 MPa) failure occurs at the notch root (Point A), where the fatigue amplitude is largest (±180 MPa). At lower notch root mean stresses (550, 420 and 350 MPa), failure occurs sub-surface about 1.6 mm below the notch (point B) despite the smaller fatigue amplitude because of tensile residual stress located there.
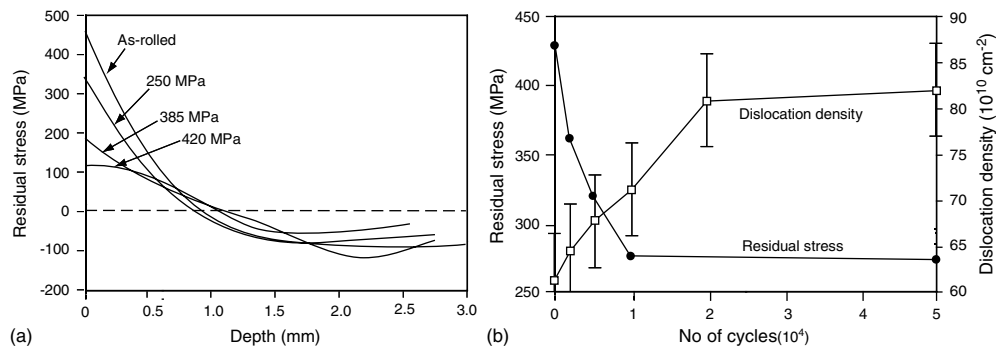
Figure 20. (*a*) Effect of different stress amplitudes after 10 000 cycles on rolled mild steel EN3b, (*b*) effect of the number of ±250 MPa cycles on residual stress and dislocation density, as measured by diffraction peak line profile analysis (Walker *et al* 1995).

6.3. Pre-stretching/stress levelling and shakedown

Mechanical deformation has been identified as a means of reducing the shape misfits between regions and thus of reducing levels of residual stress. Most methods involve either local or global plasticity. There has been interest in vibrational stress relief (VSR) procedures by which the component is vibrated at stresses below the elastic limit. It has been suggested that this procedure can relieve residual stresses and thereby lead to reduced distortion upon machining. In particular attention has been focused on weld stresses treated by VSR either post-welding (Munsi *et al* 2001b) or during welding where microstructural changes in the weld region have also been observed (Munsi *et al* 2001a). Although there have been a number of companies offering this treatment, to date documentary evidence is mixed; sometimes indicating relief, in other cases showing no effect. Mechanisms proposed for stress relief include local plastic deformation, for example in low yield stress weld metal (Aoki *et al* 2005), 'energy' absorption (Claxton and Lupton 1991) and phase transformation (Munsi *et al* 2001c). In many cases the stress amplitude applied is large ($\sim$200–400 MPa) (Walker *et al* 1995) introducing significant plastic strain (figure 20(*b*)). Indeed Sendek (1997) suggests that amplitudes of at least 50% of yield are necessary for relaxation of type I stresses, although for steels at least, lower levels may activate type II stresses due to martensitic phase changes. There is also some evidence that exposure to low frequency alternating magnetic fields can cause a levelling of the dislocation distributions and thus aid stress relief (Wu *et al* 2003).

It is indisputable that significant local or global plastic straining under external loading can be effective at relaxing residual stress (Sauer 1964, Burdekin 1969, Smith and Garwood 1990, Prime and Hill 2002). This is because the plastic strains typically introduced by such treatments are much larger than the initial eigenstrains ($\sim$tenths of a per cent) associated with residual stresses and so largely control the final stress state. For example, the residual stresses introduced in plate as a result of the Al7050 T74 designation heat treatment (solution heat-treated at 470 °C for 1 h, water quenched and then aged for 5 h at 120 °C and at 177 °C for 10 h) are about half the quoted yield stress (414 MPa) corresponding to a maximum eigenstrain around 0.3%. The +51 Temper designation involves a uniaxial 1.5–3% stretch, and as is clear from figure 21, this largely eliminates the original eigenstrain variation by preferential plastic extension in the tensile (central) region until the stresses are approximately level across the plate (essentially no remaining eigenstrain) and the plate then stretches uniformly thereby reducing the residual stresses to a tenth of their original level on removal of the load.
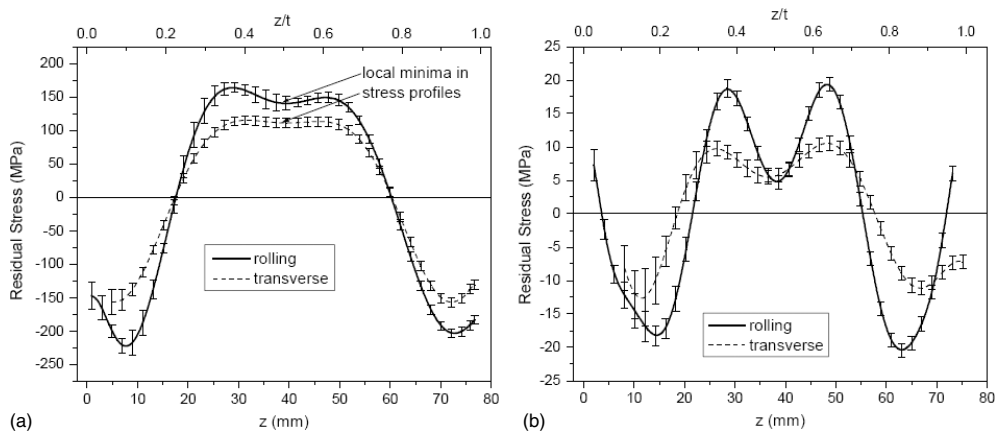
Figure 21. Residual stresses in 7050-T74 Al plate in the rolling and transverse directions (*a*) prior to and (*b*) after a stress relief stretch as measured by the crack compliance technique (Prime and Hill 2002). Note the different stress scales used in (*a*) and (*b*).
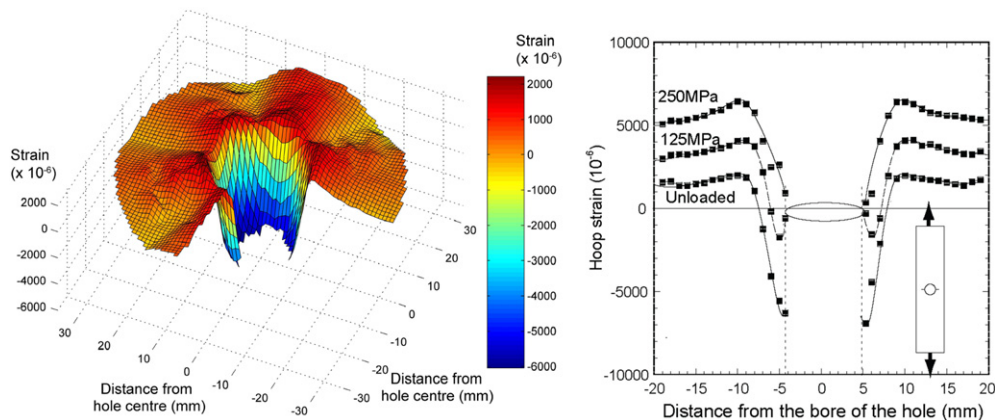

Figure 22. (*a*) Residual strains around a 4% cold expanded 12 mm hole (quarter not shown for clarity) in an 11 mm thick 7010-T7651Al plate measured by synchrotron diffraction at the ESRF (the 6-fold symmetry may be due to texture in the plate—courtesy P J Webster and D J Hughes), (*b*) Hoop strains measured laterally from the bore by synchrotron diffraction in a pre-cracked 4% cold expanded specimen (shown inset) unloaded, moderately loaded (125 MPa) and heavily loaded (250 MPa) showing the cracks to be held closed at 125 MPa (Stefanescu *et al* 2004).

Beneficial long-range residual stresses can be introduced by non-uniform plastic deformation using processes such as autofrettage for gun barrels (Hearn 1977, Webster and Ezeilo 2001), cold-hole expansion of fastener holes (Stefanescu *et al* 2004), over-pressurizing pressure vessels (Leggatt and Davey 1988), etc. All are based around the same principle; namely to permanently enlarge a hole or cavity such that plastically deformed material is constrained by neighbouring elastically deformed material thereby creating a compressive hoop stress on the misfitting region local to the cavity (figure 22(*a*)). The compressive residual stress limits the extent of tensile loading experienced in-service by the material around the cavity thereby inhibiting the nucleation and growth of fatigue cracks (see figure 22(*b*)).

Local plastic deformation can alter the residual stress state during fatigue cycling and this must be taken into account when predicting life. A good example is provided by the shakedown
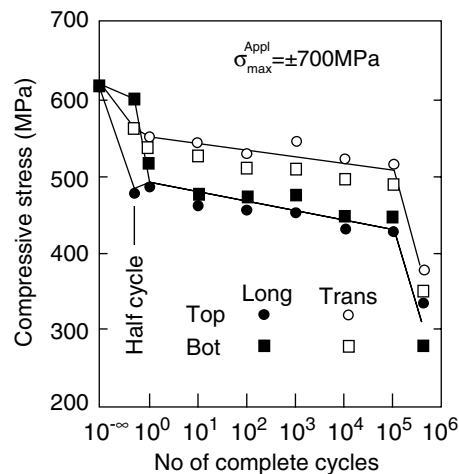
Figure 23. The effect of bending fatigue on the residual stress introduced into AISI 4140 steel by peening. During the first half cycle the top surface was loaded in longitudinal compression to 700 MPa; the bottom in tension to the same load.

of peening induced compressive stresses during cycles which include a compressive loading phase. As shown in figure 7 peening can introduce compressive in-plane stresses approaching the yield stress, and this combined with the Bauschinger effect (a tendency of a lowering of the yield stress upon reversing the direction of loading), can mean that a relatively low applied compressive stress can cause local plasticity in the near surface region (Holzapfel *et al* 1998). This reduces the misfit and thereby the residual stress during the compressive part of the first cycle (see figure 23). Cao *et al* (1994) building on the work by Kodama (1972) identified two distinct stages for the relaxation. The first stage has been termed previously 'elastic shakedown' and it occurs over the first loading cycle in figure 23. It arises because the residual stresses combine with the applied stresses to cause local plastic yielding. Holzapfel (Holzapfel *et al* 1998) also noted that the extent of in-plane stress relaxation was greater parallel to the applied load than perpendicular to it. The second stage is characterized by a slow decrease of the residual stress, and has been ascribed in part to cyclic softening. Analytical (Holzapfel *et al* 1998, Zhuang and Halford 2001) and numerical (Meguid *et al* 2005) models to describe the plastic relaxation have been developed for the fatigue of shot peening stresses.

6.4. Misfit management for stress control

As we have seen many processes generate the plastic misfits (eigenstrains) that cause residual stress. By understanding how they are generated, in certain circumstances it is possible to prevent such misfits arising. A good example of this is the management of the misfits generated during welding by thermal or mechanical tensioning to produce low residual stress welds. It has long been known that thermal and mechanical tensioning techniques can reduce residual stresses and the tendency for buckling. The first application of temperature gradients to achieve reduced residual stresses was probably by Greene and Holzbaur (1946) on longitudinal butt welds in ship hull structures in 1946. The basic principles behind weld tensioning may be summarized as follows. The tensile residual stress peak usually found in the vicinity of the weld line (e.g. figure 16) is produced during cooling of the weld and arises from the compressive plastic flow local to the weld zone that occurs when it is much hotter than the parent material
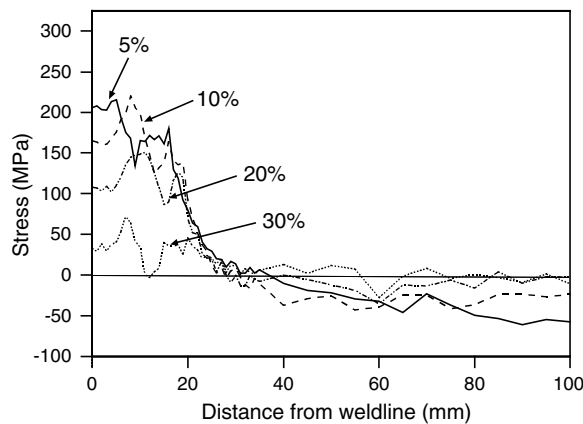
Figure 24. Longitudinal residual stress profiles at the mid-length of a friction stir weld between 1 m long Al7449 12 mm thick plates, as a function of applied tensioning level (% of RT yield stress) determined using high energy x-ray diffraction. Note for reasons of clarity the full width (153 mm) of the plates is not shown (Altenkirch *et al* 2007).

(see above). All tensioning methods rely on controlling the accumulation of this plastic misfit. A number of thermal techniques have been proposed including global heating (Burak *et al* 1977), localized cooling, referred to as heat-sink welding (HSW) (Barber *et al* 1981, Yang *et al* 2000) and localized heating (McGuire and Groom 1979, Michaleris and Sun 1997, Dydo *et al* 1998, Dydo and Cheng 1999, Dull *et al* 2001). Mechanical tensioning systems have also been used, for example, Yang *et al* (1998) used a pair of rollers placed either sides of the weld to mechanically compress the weld locally on cooling, reducing both residual stress and buckling distortion, while Altenkirch *et al* (2007) have studied global tensioning during welding to reduce the stresses (figure 24).

7. Effect of residual stress on failure

Just as residual stresses can operate over a range of scales, from below the grain scale to the scale of the complete structure, failure can also occur at the materials level, or at the full structural level. The former tends to be associated with the micromechanisms of failure at the microstructural scale and is the focus of the materials scientist, the latter associated with structural integrity at the continuum level and lies within the domain of the materials or structural engineer. For example, the nucleation of cavities at elevated temperature under creep driven by residual stress is a materials failure mechanism (see section 7.5), only when many cavities have linked up to form a long crack does it threaten to lead to structural failure. In fact in section 7.3 cracks are categorized either as short microstructurally dependent cracks, or long cracks described by continuum engineering fracture mechanics. As discussed below, short range (type II or III) residual stresses can combine with materials microstructural influences to initiate and seriously accelerate the growth of short cracks. These short cracks tend to be precursors to larger cracks that are the concern of the structural failure assessment approaches covered in section 8. As discussed below, for composites and smart materials, failure at the materials level can lead to significant changes in the structural performance. In the former case for example, fibre/matrix interfacial debonding, if correctly engineered, can significantly improve the fatigue crack resistance (section 7.3). For shape memory based actuators, increasing irreversibility of the transformation with cycling, can significantly degrade their

response (section 7.4). As a consequence, performance optimization is dependent on a good knowledge of both the likely residual stresses and the basic materials physics and engineering across the relevant microstructural and continuum scales.

7.1. Plastic collapse

In simple terms plastic collapse occurs when the stress exceeds the yield criterion over a sub-domain of the component. Engineers tend to define primary and secondary stresses based on whether they affect structural plastic collapse. The former are required to satisfy equilibrium externally (Roche 1989) and arise from imposed loading, including dead weights, internal pressures, etc although very long-range residual stresses such as fit-up stresses in pipework are sometimes included. Secondary stresses on the other hand are shorter range stresses (weld residual stresses, etc) caused by misfit (eigen) strains within the body. Upon loading to plastic collapse primary stresses are redistributed, but not relieved. In contrast during general yielding, large scale plastic deformation tends to overwrite the eigenstrains associated with the secondary stresses. As a result secondary stresses do not contribute to plastic collapse (Lidbury 1984). It should be noted that in certain cases residual stresses which are self-equilibrating over the entire structure may still result in plastic collapse in the net section around a crack-like flaw. This can occur when the flaw is small compared with the spatial extent (L_o) of the residual stress distribution, or there is significant elastic follow-up (see below) from the surrounding structure. In these cases, the residual stress should be treated as a primary stress.

7.2. Fracture

Common to all fast fractures is the catastrophic propagation of a crack from an initial microscopic defect or flaw. Historically, Griffith (1920) made a major step forwards when he realized that rather than consider the stress field around the tip of a growing crack (which is infinite anyway for a perfectly sharp crack in an elastic medium) it is more helpful to consider the energy associated with crack propagation. For a crack length $2a$ in the centre of a plate thickness t under a far-field mode I[1] (one) crack opening stress σ_∞, as the crack grows strain energy, $U (= -C \cdot t \cdot \sigma_\infty^2 \pi a^2 / E')$, is released, but in forming the crack energy, $S (= 2G \cdot t \cdot a)$, must be expended, where E' is the Young's modulus, E, under plane stress conditions ($\sigma_{zz} = 0$) and $E/(1 - \nu^2)$ under plane strain conditions ($\varepsilon_{zz} = 0$). G, the energy to create unit area of crack, is a material property, which for glass is very small ($\sim 15\,\mathrm{J\,m^{-2}}$), essentially equal to the surface energy required to create the new surface, compared with copper ($\sim 10^6\,\mathrm{J\,m^{-2}}$) which absorbs a lot of energy by local plasticity as the crack grows (Ashby and Jones 1980). For a small crack, the energy released will be less than the energy absorbed and the crack will be stable. As the crack extends the quadratic dependence of the strain energy means that there is a critical crack length at which the energy release rate (per unit increase of crack area) is equal to the rate of release of stored elastic strain energy.

$$\frac{\partial S}{\partial a} + \frac{\partial U}{\partial a} = 0 \qquad \text{giving} \qquad 2G_c = C \frac{\sigma_\infty^2 \pi a_c}{E'}. \tag{13}$$

At this point the crack becomes critical and the crack will grow catastrophically under this stress level. The energy release rate per unit area of crack created at this point is defined as the critical energy release rate or toughness, G_c and a_c the critical flaw size for the applied stress. From a design viewpoint one might ensure that the working stress is sufficiently small that the

---

[1] The I indicates mode I loading; i.e. a (crack opening) load acting normal (along y) to the crack faces.

critical flaw size is well within detectable limits by NDT. Equation (13) leads to

$$Y\sigma_\infty\sqrt{\pi a_c} = \sqrt{E'G_c}, \tag{14}$$

where Y is a geometrical factor (quoted in handbooks (Tada *et al* 1985, Fett and Munz 1997)) often close to 1. The left-hand side of equation (14) gives the combination of stress and flaw size that is critical for crack growth. The right-hand side depends only on materials properties and is sometimes called the critical stress intensity factor K_c (plane stress) or K_c (plane stress) for crack growth.

Returning to the underlying stress field, Irwin (1957) employed Westergaard's analysis (1939), to express the stress field for a crack, length $2a$, at the centre of an infinitely wide plate, loaded under mode I as

$$\begin{Bmatrix} \sigma_{xx}(r,\theta) \\ \sigma_{yy}(r,\theta) \\ \sigma_{xy}(r,\theta) \end{Bmatrix} = \frac{K}{\sqrt{2\pi r}}\cos\frac{\theta}{2} \begin{Bmatrix} 1-\sin\frac{\theta}{2}\sin\frac{3\theta}{2} \\ 1+\sin\frac{\theta}{2}\sin\frac{3\theta}{2} \\ \sin\frac{\theta}{2}\cos\frac{3\theta}{2} \end{Bmatrix} + \text{(other terms)}, \tag{15}$$

where $K_I = \sigma_\infty\sqrt{\pi a}$, r is the distance from the crack-tip, θ is the angle from the x-axis (crack propagation direction) to the point r and the other terms in the series expansion are small near the crack tip. Consequently, in the vicinity of the crack (the important 'K' dominant region), the stress intensity factor, K_I, describes the linear dependency of the local stress field on the far-field stress σ_∞ and the square root dependence on the crack length. In this way the energy and stress field approaches can be brought together ($Y = 1$ for this geometry), because when K_I equals the critical stress intensity, K_{Ic}, (sometimes called the fracture toughness) crack advance will occur spontaneously.

As mentioned above, for a material displaying some ductility, plastic flow local to the crack is the largest contributor to the toughness, G_c. As a consequence, as the specimen thickness, B, increases at first the toughness increases linearly because the volume for plastic flow increases (e.g. Roylance 1996). However, the ease of yielding and hence the plastic zone radius r_p decreases as the level of multi-axial constraint increases and hence the extent of yielding is less under plane strain than plane stress;

$$r_p \approx \frac{K_I^2}{\pi\sigma_y^2} \text{ under plane stress,}$$

$$\approx \frac{K_I^2}{3\pi\sigma_y^2} \text{ under plane strain.} \tag{16}$$

This means that the plane strain fracture toughness, K_{Ic}, is smaller than that for plane stress, K_c (figure 25). The former can be regarded as a material constant and plane strain can be assumed if the plastic zone size is less than $1/25$ of the thickness ($B > 2.5 (K_{Ic}/\sigma_y)^2$). Equation (15) predicts an infinite stress at the crack tip; in order to account for stress redistribution arising from plasticity for $r < r_p$ the notional crack length can be modified to $a + r_p$ (Knott 1973).

The applicability of K_I to describe the tendency for crack advance (the basis of linear elastic fracture mechanics) extends only to situations of 'small-scale' yielding where most of the structure is elastically loaded and the plastic zone is small compared both to the size of the K dominant region (otherwise K cannot represent the stress intensity) and the uncracked ligament (otherwise plastic collapse would occur). These conditions are satisfied for the assessment of many defect scenarios. However, in cases where the plasticity preceding fracture is less than that corresponding to general yield, but cannot be classified as small-scale, researchers tend to use either a crack opening displacement approach (COD) or the J-integral (Rice 1968), which
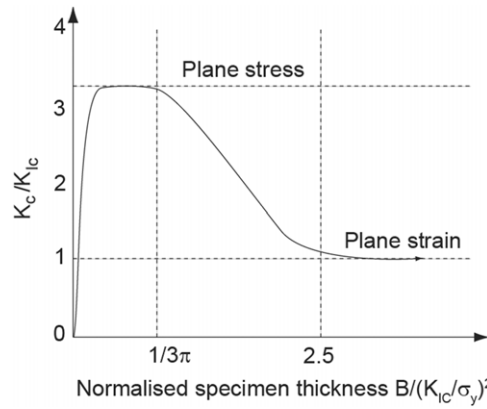
Figure 25. Schematic of the variation in fracture toughness as a function of specimen thickness, after (Said 2006).

is the rate of change of potential energy for a non-linear elastic solid per unit length of crack growth. Conveniently, J is equal to G_c for a linear elastic material.

The question of how to incorporate residual stresses when considering crack propagation is fairly simple for an essentially linear elastic brittle material:

$$K^{\text{Total}} = K^{\text{Appl}} + K^{\text{RS}} \qquad \text{if } K^{\text{Appl}} + K^{\text{RS}} \geqslant 0,$$

$$K^{\text{Total}} = 0 \qquad\qquad \text{if } K^{\text{Appl}} + K^{\text{RS}} < 0, \tag{17}$$

where K^{RS} is the stress intensity contribution from the residual stress. For example, a pane of soda glass typically has a toughness (K_{IC}) of approximately $1\,\text{MPa}\,\text{m}^{1/2}$ which means that in tension a failure strength of $50\,\text{MPa}$ would be achieved in the presence of edge cracks of size $\sim 0.3\,\text{mm}$ ($Y = 1.12$ for this geometry). If residually stressed to $-100\,\text{MPa}$ at the surface (figure 12), this would increase the failure strength to $150\,\text{MPa}$ in tension. Note that the strength of macroscopically defect-free glass is of order $2000\,\text{MPa}$ so that the balancing tensile residual stresses in the defect-free interior are unlikely to cause failure.

In the previous example the surface defects were small enough relative to the characteristic length scale (l_o—see section 2.2) of the residual stress field that it was possible to treat the residual stress at the surface as if it were an externally applied primary load (see section 5.1) and therefore essentially unaffected by the presence of the defect. In general however the presence of a crack can have a significant effect on the residual stress. This redistribution of the residual stress is important from a structural integrity assessment viewpoint. For example, one might need to know whether a residual stress field will delay or induce catastrophic failure from a given size of defect under a specific level of applied stress is reached, or to determine when a crack growing sub-critically ($a < a_c$) by a fatigue process is on the point of becoming critical.

In situations where linear elastic fracture mechanics are valid individual components of displacement, strain and stress are additive and the stress intensity for a crack in a residually stressed body can be calculated as shown in figure 26. Here K_I^{RS} can be considered as the sum of the stress intensity factor, K^{A}, arising from a residually stress free body for which crack opening tractions, $p(x)$, have been applied equal to the residual stresses, $\sigma^{\text{RS}}(x)$, that would have originally existed on the crack plane were there no crack and the stress intensity, K^{B}, for the cracked residually stressed body for which surface tractions have been applied to the crack to ensure no displacement. Since K^{B} is zero $K_I^{\text{RS}} = K^{\text{A}}$ which means that the stress
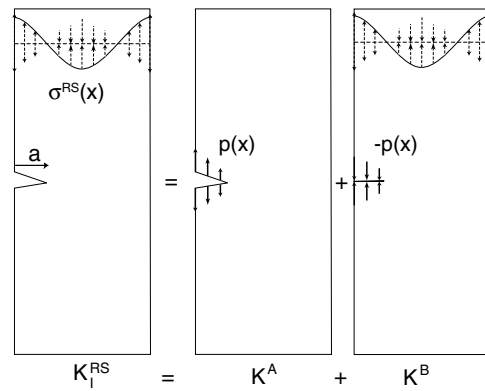
Figure 26. Determination of K_I^{RS} by means of the superposition principle where the bold arrows indicate the surface tractions applied to the crack and the dashed arrows the residual stresses, originally uniform along the length of the bar.

intensity contributed by residual stress on a crack can be calculated by replacing the stresses that originally existed along the crack plane, $\sigma^{RS}(x)$, with equivalent surface tractions, $p(x)$ acting on the crack faces (e.g. Anderson 2005). The magnitude of the stress intensity is most conveniently calculated from the crack face surface tractions using weight functions. For a through-thickness crack length a, the stress intensity factor is given by

$$K_I^{RS}(a) = \int_0^a \sigma^{RS}(x) w_p\{a, x\} \, dx, \tag{18}$$

where the weight function, $w_p\{a, x\}$, is the stress intensity arsing from a unit force applied to the crack face at x. Weight functions depend only on the geometry of the crack body and the boundary conditions. This approach is cost-effective from a non-destructive testing (NDT)/stress measurement viewpoint since it focuses only on a sub-domain so that the whole system need not be characterized. Further, it allows one to consider how one might simulate the local conditions in a large or complex component in parallel small-scale test-piece experiments for safety or lifetime assessments.

In figure 26 the body is unconstrained. In practice the body under consideration is likely to be under a mixture of imposed loading and imposed displacement constraint. A key question then becomes; 'How does the residual stress field redistribute as a crack propagates?' If the stress, or the defining eigenstrain (see section 2.1) is known everywhere this question can be answered unequivocally, but it is much harder to estimate if the stress is known only over a sub-domain. In essence this relates to the *spring effect*, also termed *elastic follow-up* (Roche 1989). This describes how the stresses redistribute locally during crack propagation (and/or local plasticity) due to the constraining effects of the remainder of the body and any external tractions. This effect is illustrated in figure 27 for three elastically extended bars. By definition, upon plastic yielding the primary load in body A remains undiminished as a result of inelastic deformations. By contrast, the secondary stress in body B is necessary to satisfy compatibility (material continuity) for an elastic material and may disappear as a result of inelastic deformation. Only in exceptional cases do residual stresses act as ideal secondary loads. As a result, it is possible to replicate the conditions locally in a sub-domain in a test-piece only if both the local residual stress redistribution and the extent of elastic follow-up (represented by the spring constant for body C in figure 27) are incorporated in the model as a function of crack growth, deformation or damage. This effect is illustrated by the influence of constraint on the stress intensity factor for a given residual stress component in figure 28(b).
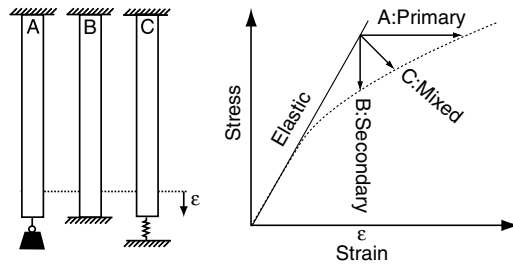
Figure 27. Classical illustration of A: primary (fixed load); B: secondary (fixed displacement) and C: realistic constraint conditions after (Roche 1989).
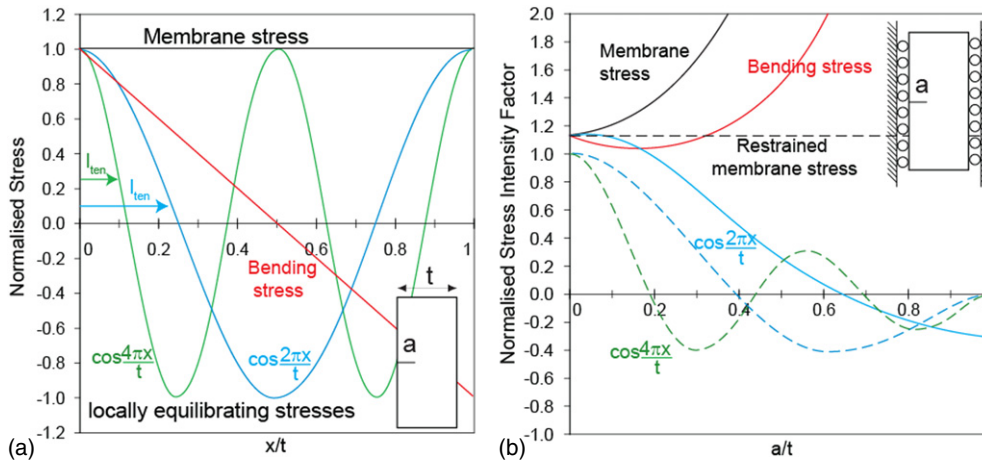

Figure 28. (*a*) Idealised membrane, bending and locally equilibrated stress profiles in a finite width plate, normalized by the peak stress and plate width, t, (*b*) stress intensity factors normalized by $\sigma_{max}\sqrt{\pi a}$ for a crack growing through thickness, for unrestrained (continuous) and restrained (dashed) remote boundary conditions (see inset) (courtesy of Bouchard). The restrained $\cos(4\pi x/t)$ stress intensity has been derived by the author using the approach outlined in (Tada 1970).

In cases where LEFM is applicable, the superposition principle means that the effects of the membrane (m), bending (b) and locally equilibrating (le) components in the sub-domain (see section 2.2) can be considered separately (Dong and Hong 2002). The significance of this lies in the fact that for a given geometry K_{Im}, and K_{Ib} can be found in handbooks (Tada *et al* 1985). Figure 28 shows the variation in K_I for the membrane, bending and two locally equilibrating components for a through-thickness edge crack growing in a thick plate, after Tada *et al* (1985). It is evident that, except at short crack lengths, the effect of restraint which affects elastic follow-up can be very important when considering how the crack-driving force changes with crack length. Stress intensity factors for the locally equilibrating part, $\sigma_{le}(x)$, are only available for simple stress distributions. The locally fluctuating part is often complex but can be deconstructed into a Fourier series. As is clear from figure 28, the influence of shorter wavelength components tend to fall off increasingly with crack length. For the cosine functions shown K_I approaches zero at approximately $1.5l_{ten}$ in the restrained case . More generally, it has been found that the K_I becomes essentially insignificant when the depth of a surface breaking crack exceeds about twice the length of the local residual stress tensile zone ($a > 2l_{ten}$) for self-equilibrating stress fields having a wavelength less than $0.8t$ or so

(Bouchard and Withers 2006). Because the shorter wavelength fluctuations in σ_{le} tend to have less effect on the stress intensity, simple representations are often sufficient. In fact the locally equilibrating component is often ignored completely and the stress intensity factor considered simply in terms of the membrane and bending components (Green and Knowles 1992, Li *et al* 2000, Stacey *et al* 2000, Lee *et al* 2005). It is clear from figure 28 that this should not be done for $a < 2l_{ten}$ unless the magnitude of the locally equilibrating stress is significantly smaller than the bending or membrane components.

For an elastic–plastic body a more complex analysis is required which cannot be evaluated by a simple linear addition of the various K terms resulting from the residual and applied stress components. In the post-yield region, finite element methods may be used to calculate the contour integral J which can be modified to include thermal/residual strains. A number of simplified assessment procedures have been developed, for example to use J defined earlier (Kumar *et al* 1985):

$$J^{Total} = \left\{\sqrt{J_{El}^{Appl}} + \sqrt{J^{RS}}\right\}^2 + J_{Pl}^{Appl}. \tag{19}$$

Here J_{El} and J_{Pl} represent the linear elastic (small-scale yielding) and fully plastic J (see Kumar *et al* 1981). This provides a reasonable estimate only for local yielding because the crack-driving force due to residual stress is taken to be a secondary stress and is thus assumed only to contribute to the elastic part of the J-integral and is taken not to change with increasing load. The tendency for the eigenstrains causing residual stress to be overwritten in cases of extensive plasticity mean that the residual stress effect on the total K or J fades as a function of load, L (see section 7.1). Schemes have been developed to address this loss of residual stress at high loads via for example a 'load interaction factor' (ρ) (Milne *et al* 1988); alternatively numerical models (Zien 1983, Lei *et al* 2000) can be used to estimate the J^{Tot}.

In all cases the length scale of the residual stress should also be considered. If it is smaller than the plastic zone, r_p (equation 16), then it is likely that the residual stress will have little effect on the fracture behaviour because crack-tip plasticity will obliterate the underlying eigenstrains.

7.3. Fatigue and thermal fatigue

Fatigue is the deleterious change in properties that occurs due to the repeated application of sub-critical stresses or strains. Fatigue crack growth can be broken down into nucleation and propagation of damage (e.g. Suresh 1991). During the nucleation stage microstructural changes cause permanent damage prior to the formation of microscopic cracks. The propagation stage begins once these microscopic flaws have grown and coalesced to form dominant macroscopic cracks. These may then propagate stably prior to rapid growth leading to fast fracture. In practice the extent of the nucleation stage is rather difficult to define; it is most easily described as encompassing all the damage and crack growth events that occur below the sensitivity threshold of NDT (1 mm say). This stage is taken to include; microstructurally small flaws having the microstructural scale (e.g. grain size), mechanically small flaws comparable to the near-tip plasticity, physically small cracks that are too small to detect by NDT but larger than the crack-tip plasticity; and finally chemically small cracks that might be expected to conform to LEFM, but below a given crack size grow anomalously due to scale dependent environmental stress corrosion effects (Suresh and Ritchie 1984). The key point is that all these short cracks propagate at rates faster than would be expected under LEFM. These cracks apparently deviate from the principle of similitude, namely the idea that the crack-tip conditions can be uniquely defined by the stress intensity factor whatever the size of the sample. This principle is fundamental to the transfer of results on the test-piece to the engineering structure.

They deviate because as short cracks they can take advantage of local microstructural or environmental conditions favouring crack advance, for example, for short cracks crack growth may be accelerated due to locally high type II stresses (section 2.2) not accounted for in a continuum LEFM approach.

For convenience fatigue is divided into two types (Ashby and Jones 1980), low cycle fatigue (LCF) and high cycle fatigue (HCF). LCF describes fatigue at stresses above the yield point and typically involves less than 10 000 cycles to failure. This usually occurs during cycling controlled by the imposed total strain, such as the thermal cycling of a constrained structure. Analogous to the static high load case, residual stress often has little effect on LCF life as the eigenstrains responsible for the residual stresses tend to be drowned-out within the first cycle or so by the large amplitude of the oscillating plastic strains. This is exemplified by a reduction of 70% of the compressive residual stress introduced by deep rolling after half the fatigue life under LCF ($R = -1$; $\sigma_{max} = 320$ MPa) for 304 stainless steel having yield, $\sigma_{0.2}$, and ultimate tensile, σ_{uts}, stresses of 245 and 650 MPa, respectively (Altenberger *et al* 1999) and almost complete relaxation of the residual stresses introduced by shot peening in SAE 1045 ferritic steel ($R = -1$; $\sigma_{max} = 450$ MPa) with ($\sigma_{0.2} = 480$, $\sigma_{uts} = 740$ MPa) (Martin *et al* 1998).

HCF involves larger numbers of cycles at stresses that would not of their own be sufficient for plastic straining to occur. HCF is generally stress controlled and includes rotating or vibrating systems. It can be very sensitive to residual stress. Just as K_I is a key parameter for assessing the likelihood of static fracture, the stress intensity range, $\Delta K_I = K_{Imax} - K_{Imin}$, is important for fatigue, as well as K_{max} and load ratio $R = \sigma_{min}/\sigma_{max}$.

Large engineering structures usually contain cracks (or are assumed to contain cracks just below the minimum detectable size), defects or stress concentrators. In such circumstances, one needs to know how many cycles, that is how long in time, it will take for one of these cracks to grow to such an extent that catastrophic fracture can occur according to (equation (14)). The crack growth rate per cycle, da/dN, versus $\log(\Delta K)$ has been found to have a sigmoidal form comprising three distinct stages; I near threshold, ΔK^{th}, that is ΔK is just large enough to propagate a fatigue crack (this regime is strongly dependent on R ratio), II a linear region described as the Paris regime (Paris and Erdogan 1963) and governed by equations (20*a*)

$$\frac{da}{dN} = A(\Delta K)^m, \tag{20a}$$

where A and m are constants dependent on stress ratio, R, microstructure and the environment. Beyond this linear region, stage III corresponds to a 'high growth' rate regime sensitive to K_{max} as the conditions for static fracture are approached. Traditionally much attention is concentrated on stage II because once a crack has initiated much of the useable fatigue life of a component will be in stage II, since crack growth is typically too rapid to tolerate in stage III. Figure 29(*a*) demonstrates that a macro residual stress changes R and K_{max}, but does not normally affect ΔK (case A). However, if the residual stress is sufficient for the crack faces to come into contact over part of the fatigue cycle, then the crack-tip stress intensity will be partially shielded from further changes in the applied loading. Finite element modelling work (Beghini and Bertini 1990, Korsunsky and Withers 1997) suggests that depending on the form and magnitude of the compressive residual stress field, the crack faces come into increasing contact gradually below some applied K^{Appl} value, but that once contact is made the stress at the crack tip varies little with changing externally applied load. As a result an adequate representation of the range of stress experienced at the crack tip can be obtained by setting K_{min}^{Eff} to the value of K at which the crack faces start to touch. In the idealized case B plotted in figure 29(*a*) this is taken to be when $K^{Appl} + K^{RS} = 0$. Compressive residual stresses mean that residual stress induced closure effects can occur even under significant tensile applied stresses,
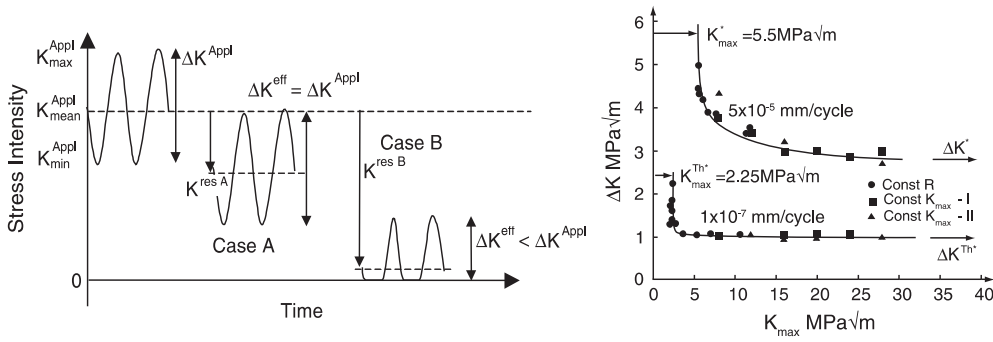
Figure 29. (*a*) Schematic showing how residual stresses directly affect the crack-tip stress intensity K_{max}^{Eff} and R ratio. Only in case B do the residual stresses affect the stress intensity range ΔK^{eff}, due to residual stress induced crack closure, this acts to limit the exposure of the crack-tip to the full applied ΔK^{Appl}, (*b*) ΔK vs K_{max} plot for Al 7475 T7351 alloy tested in the LT orientation for two crack growth rates (Sadanada *et al* 1999).

although as illustrated closure becomes less likely as the mean stress becomes more tensile. Retardation by residual stress induced closure is well illustrated by the results of Ruschau *et al* (1999) who found that laser shock peened Ti–6Al–4V aerofoils tested in bending ($R = 0.1$) as notched samples exhibited little notch sensitivity with a fatigue life twice that of the unpeened or shot peened samples. Unlike the baseline samples for which crack propagation represented just a few per cent of the total life, propagation comprised nearly 100% of fatigue life with some cracks arresting completely. This was ascribed to the fact that the deep compressive residual stresses were found to hold the crack shut for 85% of the fatigue cycle, significantly reducing ΔK^{eff}. Little benefit over the baseline was found testing at $R = 0.8$ because at the higher K_{min} levels the crack remained open throughout the cycle.

Recently, the dependency of crack growth rate on static loads, represented by K_{max}, as well as cyclic amplitude, ΔK, has been expressed (Vasudevan and Sadanada 1995, Donald *et al* 1998);

$$\frac{\mathrm{d}a}{\mathrm{d}N} = C(\Delta K)^q (K_{max})^g. \tag{20b}$$

In the same vein Vasudevan *et al* (1995, 2001) have recast the well known dependency of ΔK^{th} on R in terms of two thresholds ΔK^{th*} and K_{max}^{Th*} defining the threshold conditions for crack propagation. Further as shown in figure 29(*b*) using data for Al7475 they suggest that there are limiting ΔK^* and K_{max}^* for all crack growth rates not just at threshold (here taken to be $1 \times 10^{-7}\,\mathrm{mm\,cycle^{-1}}$). The key point from this viewpoint is that K_{max} is taken to play a role throughout crack growth. As illustrated in figure 30(*a*), Vasudevan *et al* (2001) suggest that many fatigue crack growth rate retardation effects can be explained in terms of the effect of various types of residual stress on K_{max} without the need to invoke traditional crack-tip closure mechanisms[2] to shield the crack-tip from the full stress amplitude ($\Delta K^{eff} < \Delta K^{Appl}$). This may be the dominant effect of residual stresses on fatigue when $K_{min}^{Appl} + K^{RS} > 0$ such that residual stress induced closure cannot occur.

For tension–tension fatigue, local compressive residual stresses ahead of the crack-tip arise from reverse plastic flow on unloading (figure 31(*a*)). If a tensile overload is applied the size of the compressive zone is believed to increase (Allison 1979) which has been used to explain

[2] Traditional crack closure mechanisms include crack face plasticity, asperities from oxides or corrosion, surface roughness and transformations.
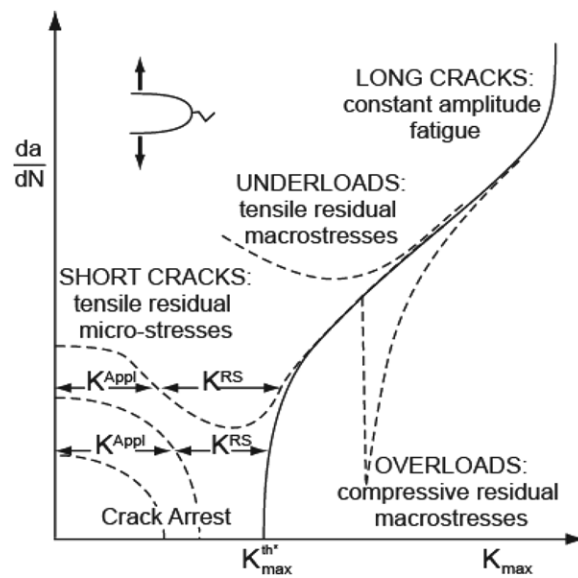
Figure 30. (*a*) Schematic illustration of the role of residual stress on crack growth rate, da/dN, for long and short cracks in terms of K_{max} after (Vasudevan *et al* 2001); a similar schematic could be drawn to show the effect of residual stress induced closure on crack growth rate via its effect on ΔK^{eff}.
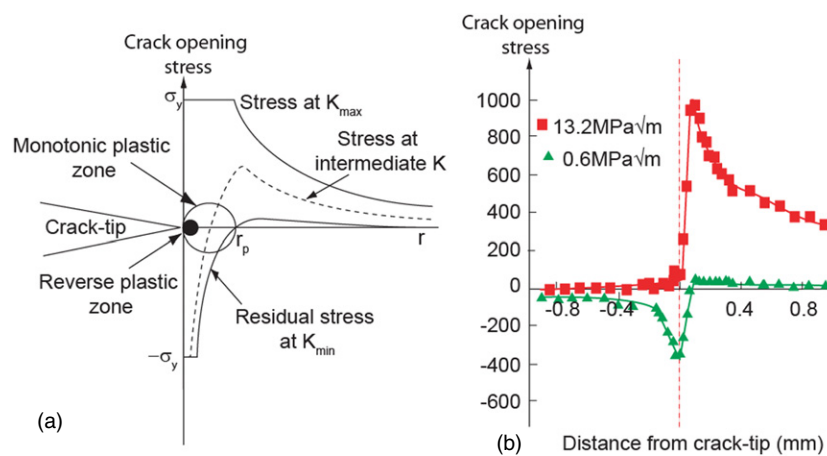
Figure 31. (*a*) Idealised sketch of the crack-tip opening stress field and forward and reverse plastic zones in fatigue and (*b*) the stress field in an as-fatigued and cracked Al compact tension specimen along the plane of the crack at $2K_{max}(=13.2\,\mathrm{MPa\,m^{1/2}})$ and $K_{min}(=0.6\,\mathrm{MPa\,m^{1/2}})$ immediately after overload measured by synchrotron diffraction using a 25 μm gauge size (Steuwer *et al* 2007).

transient retarded crack growth (figure 31) (Wheeler 1972, Garwood and Boulton 1979). This effect is exploited in the use of warm pre-stressing to increase fracture toughness of cracked components (Smith and Garwood 1990).

High spatial resolution x-ray diffraction measurements have been used to study the state of stress in the vicinity of a fatigue crack tip under plane stress (Croft *et al* 2005, Steuwer *et al* 2007). No strong evidence was found for a significant compressive residual stresses at K_{min}

Figure 32. (*a*) X-ray tomograph showing a region from a Ti matrix/140 μm SiC C-cored SCS6 fibre composite in which a fatigue crack has grown as far as ply 3. Three of the ply 1 fibres have broken (highlighted by light shading on the top face of the section), 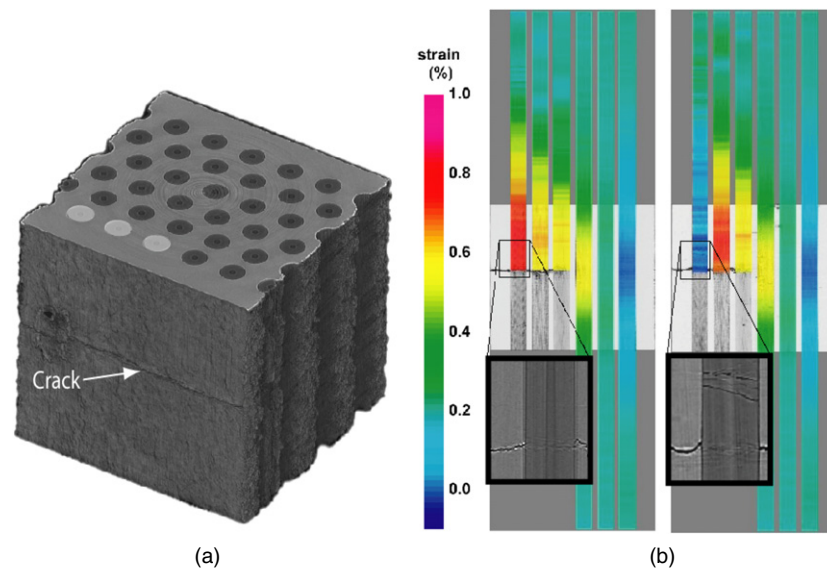(*b*) the corresponding variation in longitudinal fibre elastic strains at K_{max} measured by synchrotron diffraction across rows of fibres in which none are broken (LHS) and the ply 1 fibre is broken (RHS) superimposed on the respective tomographic slices (black and white) showing the fatigue crack morphology (Sinclair *et al* 2005).

after a normal fatigue cycle, although Croft *et al* did find evidence of type II stresses in the crack wake. However, after an overload both groups found evidence of compressive stresses behind the crack-tip indicative of the crack faces closing, as well as evidence of significant compressive stresses at the crack tip, indicative of an extensive compressive plastic zone (figure 31(*b*)). Both effects enhance fatigue resistance by shielding the crack tip from the full range of the applied stress intensity as indicated in case B of figure 29(*a*) and the latter lowers K_{max}. The dominant mechanism is the subject of some debate especially as the retardation effect can persist even after the crack has grown through the residually over-stressed zone (Suresh 1983).

With regard to crack propagation, unless the crack-tip plastic zone, r_p, is smaller than the characteristic length, l_0^{II}, the eigenstrains causing type II and type III stresses will tend to be drowned-out by crack-tip plastic strain. As a result, except for microstructurally short cracks, only type I residual stresses are normally considered from a fatigue viewpoint (figure 30(*a*)).

Type II residual and internal stresses can be important in multiphase materials because one phase may act to hold open or closed a crack growing through the other phase, even though the residual macrostress is zero. For long fibre unidirectional Ti/SiC metal matrix composites for example, tensile thermal matrix stresses and compressive fibre stresses tend to open a crack growing through the matrix. In contrast, under an applied load the unbroken bridging fibres will tend to hold the crack closed thereby limiting the effective crack-tip stress intensity range ΔK^{eff} experienced by the crack tip. Here the fibre matrix interface is engineered to allow the fibres to slide as the matrix crack reaches them such that the crack can propagate without the fibre stress rising sufficiently locally for fibre fracture to occur (figure 32). As the crack passes each ply the extent of fibre bridging increasingly shields the crack-tip from the applied stress intensity so that unless some of the fibres start to break the crack will eventually arrest (Barney *et al* 1998).

Fatigue failure often initiates from the surface of a component and hence considerable advantage can be achieved by surface modification of the near surface residual stress. Increases in fatigue lifetimes of a factor of 10 are not uncommon in materials containing high compressive near surface stresses, as might be introduced by peening (Nikitin *et al* 2004). In such situations a key question is the extent to which residual stress affects the nucleation and propagation of the fatigue cracks. Here it should be remembered that in many cases such as shot peening, the treatment affects the local hardness/microstructure and surface finish which can also have a strong effect on the nucleation of surface cracks making it difficult to quantify the effect of residual stress alone. The evidence for compressive stresses delaying and even arresting propagation is less ambiguous (e.g. Ruschau *et al* 1999). De los Rios *et al* (1995) found for 316 stainless that both initiation and growth were delayed by shot peening although initiation was the more affected, with propagation becoming increasingly important at high stresses and low fatigue lifetimes. However no attempt was made to separate the microstructural and stress effects on initiation. In common with Ruschau *et al* (1999) who looked at fatigue of laser peened materials (see above), Bernardt *et al* (1995) found propagation rather than nucleation to be most strongly retarded by cold-hole expansion.

Contact fatigue is an umbrella term that includes a wide range of contact induced surface modifying processes, including fretting, sliding contact, rolling contact, conforming contact etc. In many cases the tolerance to such processes can be increased by the prior introduction of compressive near surface residual stresses. However, contact fatigue processes will tend to introduce or modify the near surface eigenstrain by local plasticity. If the plastically affected depth is greater than the depth of the original eigenstrain then the former may drown out the latter which is typically tenths of a per cent. As a consequence it is important that the protective residual stress process introduces compressive stresses to a greater depth than is modified by the contact process so that the compressive residual stress is relatively stable and will offer protection against the propagation of fatigue cracks. From this standpoint, laser peening and deep rolling are attractive because they can introduce compressive stresses to depths greater than a millimetre (King *et al* 2006). This greater depth also confers a greater resistance to foreign object damage (Prevey *et al* 2001). It should be remembered that not all contact situations are detrimental. One area where contact fatigue introduces beneficial compressive residual stresses is on the surface of railway rails (Kelleher *et al* 2005).

7.4. Transformation fatigue of smart structures

Recently there has been considerable interest in the use of transforming materials, such as ferroelectrics and shape memory materials for actuators and smart devices. In such cases the component is repeatedly cycled between states and the residual stresses repeatedly relieved and regenerated. Eggeler *et al* (2004), distinguished between structural and functional fatigue. The former encompasses microstructural damage that accumulates during cyclic loading and eventually leads to fatigue failure. The term 'functional fatigue' indicates degradation of the shape memory effects. Functional fatigue is associated with an increase of residual strain (with plastic and pseudo-plastic components) which corresponds to an incomplete reverse transformation. The structural fatigue of pseudo-elastic shape memory alloys is governed by the initiation and growth of surface cracks. These materials are damage tolerant because the stress induced transformation limits stresses and thus stress intensity factors which drive crack growth. Fatigue in ferroelectric actuator materials has also been studied; significant effects were found once the electric loading approached the coercive field (Lupascu and Rodel 2005).

In other systems, notably transformation toughened ceramics the transformation is used once only to achieve inelastic deformation near the crack-tip. For partially stabilized zirconia
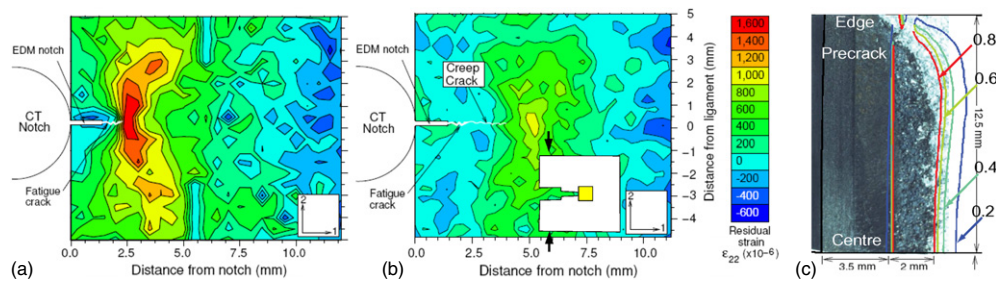
Figure 33. (*a*) Maps of the crack opening residual elastic strains across a stainless steel specimen fatigue pre-cracked to 3.5 mm (inset with scan area marked in yellow) before (LHS) and after (RHS) a 4500 h of thermal exposure at 550 °C measured by synchrotron diffraction, (*b*) comparison of the fracture surface with finite element predictions of creep cavitation damage level after thermal exposure, where 1 indicates the initiation of a creep crack (Turski *et al* 2007). Note that creep damage does not occur near the sample edge because of the lack of hydrostatic constraint.

the fatigue enhancement depends on a combination of shear and dilatational strain achieved by the tetragonal to monoclinic transformation (Garvie *et al* 1975). The shear is analogous to plastic shear whilst the dilatation introduces compressive residual stresses near the crack (where the stresses are highest) that might cause residual stress induced crack closure thereby reducing ΔK, or simply reduce K_{max}.

7.5. Creep cavitation cracking

Creep, is the inelastic deformation under load of materials over long periods, that would cause only elastic deformation if imposed for short periods. This is an important deformation mechanism at elevated temperatures. If the accumulated creep strains exhaust the creep ductility of the material, cracks will initiate. The failure mode is often characterized by the growth of cavities on grain boundaries (Bouchard *et al* 2004). Welds and the adjacent heat affected parent material are generally the regions most susceptible to creep continuum damage in fabricated steel structures. Creep strain and ultimately cracking can be driven by residual stresses, for example, as a means of thermal relaxation of weld residual stress in areas with poor material creep ductility at the operating temperature and creep deformation rate. In this context a highly tri-axial stress state—such as can be present in certain weld types—can reduce the creep ductility relative to the uniaxial response substantially. The occurrence of so called reheat cracking has been detected in welded AISI Type 316H austenitic stainless steel components operating at elevated temperatures and pressures in the boilers of UK advanced gas cooled nuclear reactor plants (Coleman *et al* 1998). Turski *et al* (2007) studied this using a pre-strained compact tension style 316H stainless steel sample (inset in figure 33(*a*)) to generate a tensile residual stress prior to introducing a 3.5 mm fatigue 'pre-crack'. Upon exposure to 550 °C for 4500 h significant stress relaxation was observed to occur by creep cavitation with no external load applied (figure 33(*b*)). Good agreement was found with the damage levels predicted by FE (figure 33(*c*) made on the basis of a stress relaxation and creep ductility exhaustion model.

7.6. Stress corrosion

It is commonly the case that aqueous exposure in combination with otherwise benign levels of applied stress can cause serious cracking to occur, often intergranularly. Stress corrosion
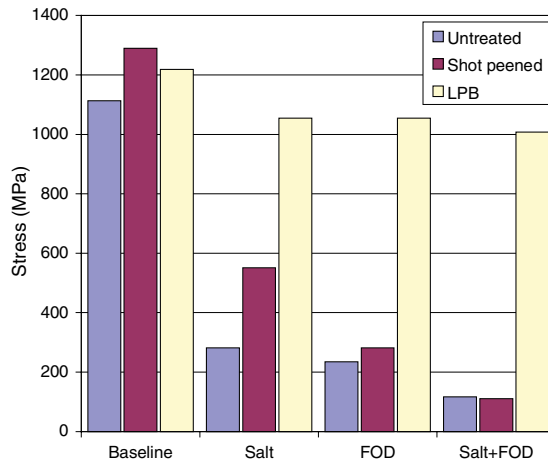
Figure 34. Fatigue strength at 10^7 cycles for 0.5 mm notched SCC study of 300 M steel in the presence of a neutral 3.5% salt solution for untreated, shot peened and low plasticity burnished conditions (Prevéy *et al* 2005).

cracking is a particular worry for the oil, petrochemical and power generation industries. As a near surface phenomena, stress corrosion is particularly amenable to prevention by control of the near surface stress state and significant ($\times 100$ (Prevey and Cammett 2004)) increases in the resistance to stress corrosion have been achieved by the various peening methods. Figure 34 shows that in contrast to shot peening, low plasticity burnishing (introducing 1.25 mm deep compressive stresses) was found to confer good resistance under 0.5 mm notched SCC and foreign object damage (FOD) testing (Prevéy *et al* 2005). As a microstructural mechanism, it is possible that both type I and type II stresses can contribute to stress corrosion cracking.

8. Assessment of structural integrity

8.1. Assessment strategies and codes

Structural integrity has been described[3] as the 'science and technology of the margin between safety and disaster' of engineering structures. In essence it is the demonstration to an appropriate level of confidence of the fitness for service of a particular component, structure or plant. Several codes and procedures have been defined for its assessment. The fracture assessment procedure summarized in BS 7910:1999 is based on the use of the failure assessment diagram (FAD). The FAD provides a simple way of considering the competing tendencies for fracture (vertical axis) due to the stress intensity ($K_{\mathrm{I}}^{\mathrm{Total}}$) and plastic collapse (horizontal axis) due to the load (L). The respective axes, K_r, and, L_r, of the FAD (figure 35) are normalized by the appropriate material toughness (K_{Ic} under linear elastic fracture conditions) and the plastic limit load of the cracked structure, L_{L}. The boundary between safe and unsafe conditions can be defined in a number of ways:

Option 1 is to use a general curve given by (Milne *et al* 1988):

$$K_r = (1 - 0.14L_r^2)[0.3 + 0.7\exp(-0.65L_r^6)] \qquad \text{for } L_r \leqslant L_r^{\max}$$
$$K_r = 0 \qquad \text{for } L_r > L_r^{\max}. \tag{21}$$

Option 2 is to use a material specific curve.

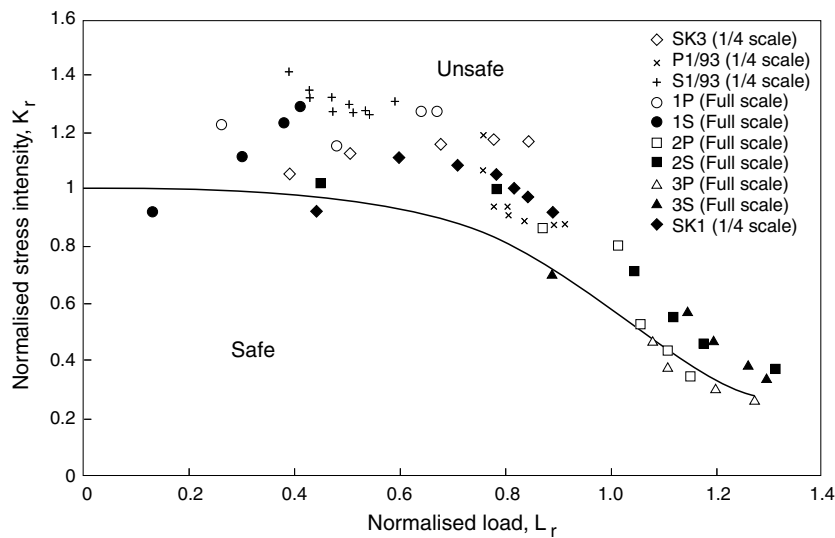[3] Dr S G Roberts, University of Oxford at an EPSRC Structural Integrity Workshop, 2004.

Figure 35. FAD diagram for centre cracked plate Al specimens with (S) and without (P) various levels of residual stress (1S: $\sigma_{max}^{RS} = 23\%\sigma_y$, 2S: $\sigma_{max}^{RS} = 44\%\sigma_y$, 3S: $\sigma_{max}^{RS} = 48\%\sigma_y$, SK3: $\sigma_{max}^{RS} = 16\%\sigma_y$, S1/93: $\sigma_{max}^{RS} = 57\%g\sigma_y$) calculated using option 1 (Stacey *et al* 2000).

The cut-off for plastic collapse, L_r^{max}, is often taken as $1/2(\sigma_y + \sigma_{uts})/\sigma_y$ except where higher values can be justified (Milne *et al* 1988).

Secondary stresses (including many types of residual stress) by definition only affect the vertical position (K_r) on the FAD (equation (21)). As discussed in section 7.2, methods for incorporating the effects of extensive plasticity at high L_r on K_r have been developed (Milne *et al* 1988, Stacey *et al* 2000) which bring K^{Total} (or J^{Total}) closer to K^{Appl} as L_r becomes large. This is because the relatively small eigenstrains causing the residual stress tend to become overwritten by larger local plastic strains.

Three assessment levels for incorporating residual stress are used, in order of increasing sophistication and prior knowledge and hence decreasing conservatism (Stacey *et al* 2000).

Level 1 can best be thought of as a screening procedure. It entails making very conservative assumptions about the treatment of the applied and residual stresses. For example, an as-welded residual stress distribution is normally assumed to be a membrane stress equal to the yield strength.
Level 2 is the usual assessment method for structural applications in cases where the residual stress profile is known or can be estimated. The level 2 method gives realistic predictions for situations, where ductile tearing is limited and involves predicting the total K^{Total} taking into account applied and residual stresses for example using equations (18) and (19).
Level 3 this procedure is appropriate to ductile materials which exhibit stable tearing and can involve a full J-integral numerical analysis (see section 7.2), to yield a plot of K_r versus L_r.

Data on residual stresses may be obtained from published literature, measurements or numerical modelling. Standard residual stress distributions for common welded joint geometries are included in BS 7910:1999 Annex Q, British Energy R6 Rev.4 section IV.4 and API 579 appendix E. These distributions were obtained by fitting upper bounds to published data, and are available for butt welds, T-joints, girth welds in tubes and repair welds and have also been expressed as mathematical formulations (Stacey *et al* 2000). Guidelines for the effect

of post-weld heat treatment are also given (BS 7910:1999). Test results are plotted against the R6 option 1 FAD in figure 35 for a centre cracked Al plate containing various levels of residual stress (% of yield stress). The figure shows that, in general, conservative predictions were obtained with failure occurring on the unsafe side of the FAD curve.

The R6 FAD is based on elastic-perfectly plastic behaviour. As such it is conservative for materials that harden with straining. The Electrical Power Research Institute approach involves considering elastic–plastic, J_{El}, and fully plastic, J_{Pl}, situations separately (Shih and Hutchinson 1976, Kumar *et al* 1981). J-based failure assessment diagrams analogous to figure 35 have been developed; these depend on geometry and so are more involved than the R6 procedure.

8.2. Designing against fatigue

There are two basic methods for designing with fatigue, one emphasizing nucleation, the other the propagation of fatigue cracks (Suresh 1991):

Total life approaches. Here the number of stress (or strain) denoted S, cycles to failure, denoted N, in uncracked samples is measured under prescribed conditions to give so-called S–N curves. Since crack initiation is a major fraction of the fatigue life of smooth specimens, in many cases this is equivalent to designing to prevent crack nucleation. For HCF, life is typically characterized by the stress range, whereas for lives under LCF attention has focused on the strain range. The stress life approach arose out of work by Wöhler (1860) who defined an endurance limit. This is a stress below which the component might have an infinite life (at least 10^7 cycles). Not all materials exhibit an endurance limit. The number of reversals to failure, $2N_{\text{f}}$, can often be related to the stress amplitude $\Delta\sigma$ by Basquins Law;

$$\frac{\Delta\sigma}{2}. = C_1(2N_{\text{f}})^a, \tag{22a}$$

where C_1 and a are constants, the latter varying between $-1/8$ and $-1/15$ (Ashby and Jones 1980). Residual stress effects are usually explained in terms of mean stress effects. For LCF, strain based approaches are more relevant. Here the plastic strain amplitude is related to the number of reversals via the Coffin–Manson equation:

$$\frac{\Delta\varepsilon_{\text{Pl}}}{2} = C_2(2N_{\text{f}})^b, \tag{22b}$$

where b lies around -0.5. Given that the elastic strain amplitude is given by $\Delta\varepsilon_{\text{El}} = \Delta\sigma/E$, where E is Young's modulus, then the total strain amplitude can be expressed:

$$\frac{\Delta\varepsilon_{\text{Tot}}}{2} = \frac{\Delta\varepsilon_{\text{Pl}}}{2} + \frac{\Delta\varepsilon_{\text{El}}}{2} = C_2(2N_{\text{f}})^b + \frac{C_1}{E}(2N_{\text{f}})^a. \tag{22c}$$

At short fatigue lives, plastic strain amplitude is dominant with ductility an important issue, whereas for long lives rupture strength is critical.

Defect-tolerant approaches. Here fracture mechanics is applied on the assumption that the component is inherently flawed. The maximum flaw size may be measured or a limit placed on it by the detection sensitivity. The useful life is then determined on the basis of the time to propagate such a crack predicted using empirical growth laws, until it reaches some critical size. The approach is valid for small-scale yielding.

The two methods can be applied using a safe-life approach in which the component is withdrawn from service after some fraction of the predicted life of the component. Alternatively, a fail-safe approach can be taken in which failure of the component is tolerated provided the integrity of the structure is not compromised. An example of this philosophy

is the leak-before-break approach in which pressure vessels are designed such that a crack will fully penetrate the wall and release the pressure before a defect is large enough to cause catastrophic fast fracture.

9. Summary and future directions

The last two decades has seen a marked improvement in the level to which residual stresses can be measured both near surface and at depth. This is due to the building of dedicated neutron diffraction strain measurement facilities, the emergence of third generation synchrotron sources capable of producing narrow beams of penetrating high energy x-rays, the refinement of many destructive techniques of stress measurement such as incremental and deep hole drilling and crack compliance, and a better understanding of the physics of less direct methods of stress measurement such as magnetoelastic methods. At the same time, there has been a significant improvement in the capability of computational methods to predict the generation and evolution of residual stresses during processing, assembly and through-life. Taken together these tools are greatly increasing our understanding of residual stress levels and their stability under a wide range of environmental conditions. This is enabling us to control the behaviour of a wide range of materials by tailoring the state of residual stress at the appropriate scale.

A good example is provided by the design of weld filler metals with phase transformation temperatures tailored to control the state of stress and distortion in the welded components (Yamamoto *et al* 2002). In this case synchrotron diffraction has been used to confirm the evolution of the transformation products in real-time as a function of temperature and cooling rate (Elmer *et al* 2000, Stone *et al* 2008), while neutron diffraction has been used to compare the weld residual stresses in welded joints using the new filler metals to those for conventional benchmark fillers (Francis *et al* 2007). Similarly, smart ferroelectric and shape memory materials for actuators and morphable structures are being developed with the help of the in situ measurement of phase transformation strains under magnetic, electric and applied loads.

With the development of microelectromechanical systems and nanomaterials, new measurement techniques, both destructive and non-destructive, suited to the evaluation of residual stresses at micrometre and even sub-micrometre levels will be required to understand and manipulate the behaviour of these devices. At the highest resolutions, methods in which diffraction patterns are inverted computationally can be used to derive strain information at the nanometre scale. Strain breaks the inversion symmetry giving rise to fine detail at each diffraction spot (Pfeifer *et al* 2006). For example the 2D variation in strain in a 100 nm by 1 μm single crystal Si of an electronic device has been mapped in this way to a spatial resolution of around 8 nm (Minkevich *et al* 2007).

The engineering of stress near surface is another area for the future. Recent process developments have increased the number of methods by which residual stresses can be introduced near surface over depths ranging from 10 μm to many millimetres. Often compressive near surface stresses are balanced by tension sub-surface or laterally. Both the efficacy and the longevity of the performance benefits can be affected by the depth of the compressive stress and balancing tensile regions, the stored plastic work as well as the maximum compressive stress. As a result, more work needs to be done to better understand the optimum profiles for prolonged component life under a variety of environments (fatigue, fretting, thermal exposure).

At a structural engineering level there is still a large cultural gap between those involved in residual stress measurements and those making structural integrity assessments. While the science of fracture mechanics has developed to predict the effect of measured, or presumed worst case, defects on the structural integrity of structures, the science of predicting the effect

of residual stress on structural performance is much less advanced. This is partly because up until recently the level of residual stress in a body was, except in a few cases, purely speculative. Consequently, advances in the methodology for incorporating residual stresses have not yet benefited from the advances in residual stress measurement and prediction. Consequently, it is now time that a major effort is directed at understanding how residual stresses, along with the presence of known or worst case defects combine to limit life. This is important if unnecessary conservatism is to be reduced leading to longer lives and leaner designs without compromising safety.

Finally, while it is common practise at present for potentially harmful residual stresses to be removed (stress relieved) or beneficial stresses deliberately introduced (e.g. by peening) to increase operating safety margins, it is currently rare for residual stresses to be used directly as part of lifing assessments. If residual stresses are to be intelligently exploited in the future using arguments based on structural integrity assessments that can take full value of their benefit, then it is essential that residual stress levels are known not just at start of life, but also as a function of the environmental conditions to which a component is exposed, both within and outside normal operating conditions. Non-destructive methods are particularly useful in this regard, especially those which can be made on the component in situ, as are better models for predicting the evolution of residual stress. If these challenges can be met then residual stresses can bring significant safety and economic benefits to new designs in the future.

Acknowledgments

References

API 579: *Recommended Practice for Fitness-For-Service* (Washington, DC: American Petroleum Institute)

Allen A J, Andreani C, Hutchings M T and Windsor C G 1981 Measurement of internal stress within bulk materials using neutron diffraction *NDT Int.* **15** 249–54

Allen A J, Bourke M, Dawes S, Hutchings M T and Withers P J 1992 The analysis of internal strains measured by neutron diffraction in Al/SiC MMCs *Acta Metall.* **40** 2361–73

Allison J E 1979 Measurement of crack-tip stress distributions by x-ray diffraction *Fracture Mechanics; STP 677* (Philadelphia: ASTM)

Altenberger I, Scholtes B, Martin U and Oettel H 1999 Cyclic deformation and near surface microstructures of shot peened or deep rolled austenitic stainless steel AISI 304 *Mater. Sci. Eng.* A **264** 1–16

Altenkirch J, Steuwer A, Peel M J, Richards D and Withers P J 2007 The effect of tensioning and sectioning on the development of residual stresses in AA7749 aluminium friction stir welds *Mater. Sci. Eng.* A submitted

Anderson T L 2005 *Fracture Mechanics: Fundamentals and Applications* (Boca Raton, FL: CRC Press)

Aoki S, Nishimura T and Hiroi T 2005 Reduction method for residual stress of welded joint using random vibration *Nucl. Eng. Des.* **235** 1441–5

Ashby M F 1970 The deformation of plastically non-homogeneous materials *Phil. Mag.* **21** 399–424

Ashby M F and Jones D R H 1980 *Engineering Materials—An Introduction to Their Properties and Applications* (Oxford: Pergamon)

ASME 2004 *ASME Boiler and Pressure Vessel Code* Section III, Div. 1. Rules for construction of pressure vessels (UW-40 Proceures for PWHT)

Barber T E, Brust F W, Mishler H W and Kanninen M F 1981 Controlling residual stresses by heat sink welding *Electrical Power Research Institute Report*

Barney C, Ibbotson A and Bowen P 1998 Experimental characterization of fibre failure and its influence on crack growth resistance in fibre reinforced titanium metal matrix composites *Mater. Sci. Technol.* **14** 658–68

Barsom J M 1968 Fracture of tempered glass *J. Am. Ceram. Soc.* **51** 75–8

Beghini M and Bertini L 1990 Fatigue crack propagation through residual stress fields with closure phenomena *Eng. Fract. Mech.* **36** 379–87

Beghini M, Bertini L and Raffaelli P 1994 Numerical-analysis of plasticity effects in the hole-drilling residual-stress measurement *J. Test. Eval.* **22** 522–9

Bernardt M, Bui-Quoc T and Burlat M 1995 Effect of re-coldworking on fatigue life enhancement of a fastener hole *Fatigue Fract. Eng. Mater. Struct.* **18** 765–75

Berveiller S, Inal K, Kubler R, Eberhardt A and Patoor E 2004 Experimental approach of the martensitic transformation in shape-memory alloys and TRIP steels *J. Physique IV* **115** 261–8

Bilby B A 1980 Tewksbury lecture—putting fracture to work *J. Mater. Sci.* **15** 535–56

Blaszkiewicz M, Albertin L and Junke W 1996 The eddy current technique for determining residual stresses in steels *Mater. Sci. Forum* **210** 179–85

Blodgett M P and Nagy P R 2004 Eddy current assessment of near surface residual stresses in shot peened nickel-base superalloys *J. Nondestr. Eval.* **23** 107–23

Bouchard P J and Withers P J 2007 Identification of residual stress length scales and their implications for fracture assessments *Int. J. Fract.* submitted

Bouchard P J, Withers P J, Macdonald S and Hennan R 2004 Quantification of creep cavitation damage mapping around a crack in a pressure vessel stainless steel *Acta Mater.* **52** 23–34

Burak Y I, Besedina L P, Romanchuk Y P, Kazimirov A A and Morgun V P 1977 Controlling longitudinal plastic shrinkage of metal during welding *Autom. Weld. USSR* **30** 21–4

Burdekin F M 1969 *Heat Treatment of Welded Structures* (Cambridge: The Welding Institute)

Buttle D J and Scruby C 2001 Residual stresses: measurement using magnetoelastic effects *Encyclopedia of Materials: Science and Technology* ed K H J Buschow *et al* (Oxford: Elsevier)

Buttle D J, Scruby C B, Briggs G A D and Jakubovics J P 1987 The measurement of stress in steels of varying microstructure by magnetoacoustic and Barkhausen emission *Proc. R. Soc.* A **414** 469–97

Cao W, Khadhraoui M, Brenier B, Guedou J Y and Castex L 1994 Thermomechanical relaxation of residual-stress in shot peened nickel-base superalloy *Mater. Sci. Technol.* **10** 947–54

Cheng W, Finnie I and Vardar Ö 1991 Measurement of residual stresses near the surface using the crack compliance method *J. Eng. Mater. Technol.* **113** 199–204

Cherkaoui M, Berveiller M and Sabar H 1998 Micromechanical modeling of martensitic transformation induced plasticity TRIP in austenitic single crystals *Int. J. Plast.* **14** 597–626

Cheskis H P and Heckel R W 1968 In-situ measurements of deformation behaviour of individual phases in composites by x-ray diffraction *Metal Matrix Composites* ASTM STP 438 (Philadelphia: American Society for Testing and Materials)

Clausen B, Lorentzen T, Bourke M A M and Daymond M R 1999 Lattice strain evolution during tensile loading of stainless steel *Mater. Sci. Eng.* A **259** 17–24

Claxton R A and Lupton A 1991 Vibratory stress relieving of welded fabrications *Weld. Met. Fabr.* **59** 541–4

Coleman M C, Miller D A and Stevens R A 1998 Reheat cracking strategies to assure integrity of type 316 welded components *Proc. Int. Conf. on Integrity of High Temp. Welds (London)* (London: PEP)

Covey-Crump S J, Holloway R F, Schofield P F and Daymond M R 2006 A new apparatus for measuring mechanical properties at moderate confining pressures in a neutron beamline *J. Appl. Crystallogr.* **39** 222–9

Cowley K D and Beaumont P W R 1997 The measurement and prediction of residual stresses in carbon-fibre/polymer composites *Compos. Sci. Technol.* **57** 1445–55

Croft M, Zhong Z, Jisrawi N, Zakharchenko I, Holtz R L, Skaritka J, Fast T, Sadananda K, Lakshmipathy M and Tsakalakos T 2005 Strain profiling of fatigue crack overload effects using energy dispersive x-ray diffraction *Int. J. Fatigue* **27** 1408–19

Cullity B D 1978 *Elements of X-Ray Diffraction* (Reading, MA: Addison-Wesley)

Daymond M R and Withers P J 1996 A Synchrotron radiation study of transient internal strain changes during the early stages of thermal cycling in an Al/SiC$_W$ MMC *Scr. Mater.* **35** 1229–34

De Los Rios E R, Walley A, Milan M T and Hammersley G 1995 Fatigue crack initiation and propagation on shot-peened surfaces in A316 stainless steel: I. *J. Fatigue* **17** 493–9

Donald J K, Bray G H and Bush R W 1998 Introducing the K_{max} sensitivity concept for correlating fatigue crack propagation *High Cycle Fatigue of Structural Materials* ed W O Soboyejo and T S Srivatsan (Warrendale, PA: TMS)

Dong P and Hong J K 2002 Recommendations for determining residual stresses in fitness-for-service assessment *WRC Bull.* **476** 1–61

Dull R M, Dydo J R and Russell J J 2001 Transient thermal tensioning for control of buckling distortion *82nd Annual AWS Convention (Cleveland)*

Dunand D C, Mari D, Bourke M A M and Roberts J A 1996 NiTi and NiTi-TiC composites. 4 Neutron diffraction study of twinning and shape memory recovery *Met. Mater. Trans.* A **27** 2820–36

Dydo J R, Chen Y and Cheng W 1998 Development and experimental verification of angular distortion models in welded thin panels *Defense Manufacturing Conf. (New Orleans)*

Dydo J R and Cheng W 1999 Finite element modeling of angular distortion in stiffened thin-section panels *Proc. 9th Int. Conf. on Computer Technology in Welding (Detroit)*

Eggeler G, Hornbogen E, Yawny A, Heckmann A and Wagner M 2004 Structural and functional fatigue of NiTi shape memory alloys *Mater. Sci. Eng.* A **378** 24–33

Elmer J W, Wong J and Ressler T 2000 In situ observation of phase transformations during solidification and cooling of austenitic stainless steel welds using time-resolved x-ray diffraction *Scr. Mater.* **43** 751–7

Eshelby J D 1957 The Determination of the elastic field of an ellipsoidal inclusion and related problems *Proc. R. Soc.* A **241** 376–96

Fairand B P, Williams D N, Wilcox B A and Gallaghe W J 1972 Laser shock-induced microstrutural and mechanical property changes in 7075 aluminum *J. Appl. Phys.* **43** 3893–5

Fett T and Munz D 1997 *Stress Intensity Factors and Weight Functions* (Southampton, UK: Computational Mechanics Publications)

Francis J A, Kundu S, Bhadeshia H K D H, Stone H J, Rogge R B, Withers P J and Karlsson L 2007 Transformation temperatures and welding residual stresses in ferritic steels *Proc. PVP2007 (San Antonio)*

Fry A T 2002 Residual stress measurement: XRD depth profiling using successive material removal *NPL*

Garvie R C, Hannink R H and Pascoe R T 1975 Ceramic steel? *Nature* **258** 703–4

Garwood S J and Boulton C F 1979 Cumulative damage in welded steel structures *CEGB Report*

Grant P V and Lord J D 2002 An evaluation of four hole drilling analysis techniques with respect to non-uniform residual stress fields *NPL*

Green D and Knowles J 1992 The treatment of residual stress in fracture assessment of pressure vessels *PVP Pressure Vessel Fracture, Fatigue and Life Management* (New York: ASME)

Greene T W and Holzbaur A A 1946 Controlled low-temperature stress relieving *Weld. J. Res. Suppl.* **11** 171s–85s

Griffith A A 1920 The phenomena of rupture and flow in solids *Phil. Trans. R. Soc.* A **221** 163–97

Gruver R M and Buessem W R 1971 Residual stresses in cylindrical rods as measured by dimensional changes after slotting *Am. Ceram. Soc. Bull.* **50** 749–51

Guz A N and Makhort F G 2000 The physical fundamentals of the ultrasonic nondestructive stress analysis of solids: I. *Appl. Mech.* **36** 1119–49

Hall D A, Steuwer A, Cherdhirunkorn B, Withers P J and Mori T 2005 Micromechanics of residual stress and texture development due to poling in polycrystalline ferroelectric ceramics *J. Mech. Phys. Solids* **53** 249–60

Han S, Brennan F P and Dover W D 2002 Development of the alternating current stress measurement model for magnetostriction behaviour of mild steel under orthogonal magnetic fields for stress measurement *J. Strain Anal.* **37** 21–31

Hauk V 1997 *Structural and Residual Stress Analysis by Non-destructive Methods* (Oxford: Elsevier)

Hearn E J 1977 *Mechanics of Materials* (Oxford: Pergamon)

Hill R 1952 The elastic behaviour of a crystalline aggregate *Proc. Phys. Soc. Lond.* A **65** 349

Holzapfel H, Schulze V, Vöhringer O and Macherauch E 1998 Residual stress relaxation in an AISI 4140 steel due quasistatic and cyclic loading at higher temperatures *Mater. Sci. Eng.* A **248** 9–18

Hooker V E, Aggson J R and Bickel D L 1974 *Improvements in the Three-Component Borehole Deformation Gage and Overcoring Techniques* (Washington, DC: US Department of the Interior)

Hornbogen E 2004 Thermo-mechanical fatigue of shape memory alloys *J. Mater. Sci.* **39** 385–99

Huang Y and Young R J 1994 Analysis of the fragmentation test for carbon-fibre epoxy model composites by means of Raman spectroscopy *Compos. Sci. Technol.* **52** 505–17

Huber J E and Fleck N A 2001 Multi-axial electrical switching of a ferroelectric: theory versus experiment *J. Mech. Phys. Solids* **49** 785–811

Hurrell P, Watson C T, Everett D and Bate S 2006 Review of residual stress mitigation methods for application in nuclear power plant *Proc. PVP 2006 (Vancouver, BC)*

Hutchings M T, Withers P J, Holden T M and Lorentzen T 2005 *Introduction to the Characterisation of Residual Stresses by Neutron Diffraction* (Boca Raton, FL/London: CRC Press/Taylor and Francis)

Hyde T R, Evans J T and Shaw B A 2000 Effect of stress and heat treatment on magnetic Barkhausen emission in case carburized steels *Mater. Eval.* **58** 985–90

Inoue K, Yamaguchi Y, Ohoyama K, Note R and Enami K 2002 Martensitic and magnetic transformations of Ni_2MnGa-based shape-memory alloys *Appl. Phys.* A **74** S1061–5

Irwin G R 1957 Analysis of stresses and strains near the end of a crack traversing a plate *J. Appl. Mech.* **24** 361–4

James M N 1998 Engineering materialism and structural integrity *J. Eng. Des.* **9** 329–42

Kang K J, Yao N, He M Y and Evans A G 2003 A method for in situ measurement of the residual stress in thin films by using the focused ion beam *Thin Solid Films* **443** 71–7

Kaouache B, Berveiller S, Inal K, Eberhardt A and Patoor E 2004 Stress analysis of martensitic transformation in Cu–Al–Be polycrystalline and single-crystalline shape memory alloy *Mater. Sci. Eng.* A **378** 232–7

Karaca H E, Karaman I, Lagoudas D C, Maier H J and Chumlyakov Y I 2003 Recoverable stress-induced martensitic transformation in a ferromagnetic CoNiAl alloy *Scr. Mater.* **49** 831–6

Kelleher J, Buttle D J, Mummery P M and Withers P J 2005 Mapping residual stress in railway rails *ICRS7 Mater. Sci. Forum* **490–1** 165–70

Kelleher J, Prime M B, Buttle D, Mummery P M, Webster P J, Shackleton J and Withers P J 2003 The measurement of residual stress in railway rails by diffraction and other methods *J. Neutron Res.* **11** 187–93

Kim S-B, Evans A, Shackleton J, Bruno G, Preuss M and Withers P J 2005 Stress relaxation of shot-peened Udimet 720Li under solely elevated temperature exposure and under isothermal fatigue *Mater. Met. Trans.* A **36** 3041–53

King A, Steuwer A, Woodward C and Withers P J 2006 Effects of fatigue and fretting on residual stresses introduced by laser shock peening *Mater. Sci. Eng.* A **435–6** 12–18

Kistler S S 1962 Stresses in glass produced by nonuniform exchange of monovalent ions *J. Am. Ceram. Soc.* **45** 59–68

Knott J F 1973 *Fundamentals of Fracture Mechanics* (London: Butterworths)

Kodama S 1972 The behavior of residual stress during fatigue stress cycles *Proc. Int. Conf. on Mechanical Behavior of Metals II (Kyoto)* (Kyoto: Society of Materials Science)

Korsunsky A M, Regino G and Nowell D 2004 Variational determination of eigenstrain sources of residual stress: I. *Conf. on Computational and Experimental Engineering and Science (Madeira)*

Korsunsky A M and Withers P J 1997 Investigation of residual stress induced crack closure and its effects on fatigue in metal matrix composites *Key Eng. Mater.* **127** 1183–90

Kröner E 1958 Berechnung der elastischen konstanten des vielkristalls aus den konstanten des einkristalls *Z. Phys.* **151** 404–18

Kumar A and Debroy T 2004 Guaranteed fillet weld geometry from heat transfer model and multivariable optimization *Int. J. Heat Mass Transfer* **47** 5793–806

Kumar V, German M D and Shih C F 1981 An engineering approach for elastic–plastic fracture analysis *Electrical Power Research Institute Report* Palo Alto

Kumar V, Schumacher B I and German M D 1985 Development of a procedure for incorporating secondary stresses in the engineering approach *Electric Power Research Institute Report*

Lebrun J L, Gergaud P, Ji V and Belassel M 1995 Interests of synchrotron-radiation for internal-stress analysis *J. Physique IV* **4** 265–8

Lee H Y, Nikbin K M and O'Dowd N P 2005 A generic approach for a linear elastic fracture mechanics analysis of components containing residual stress *Int. J. Pressure Vessels Piping* **82** 797–806

Leggatt R H and Davey T G 1988 Measurements of the reduction due to proof loads of residual stresses in simulated pressure vessels *Mechanical Relaxation of Residual Stresses* (Philadelphia: ASTM)

Leggatt R H, Smith D J, Smith S D and Faure F 1996 Development and experimental validation of the deep hole method for residual stress measurement *J. Strain Anal. Eng. Des.* **31** 177–86

Lei Y, O'Dowd N P and Webster G A 2000 Fracture mechanics analysis of a crack in a residual stress field *Int. J. Fract.* **106** 195–216

Lester H H and Aborn R H 1925 Behaviour under stress of iron crystal in steel *Army Ordnance* **6** 120–7

Lester H H and Aborn R H 1925 Behaviour under stress of iron crystal in steel *Army Ordnance* **6** 200–7

Lester H H and Aborn R H 1925 Behaviour under stress of iron crystal in steel *Army Ordnance* **6** 283–7

Lester H H and Aborn R H 1925 Behaviour under stress of iron crystal in steel *Army Ordnance* **6** 364–9

Li J Y, Rogan R C, Ustundag E and Bhattacharya K 2005 Domain switching in polycrystalline ferroelectric ceramics *Nat. Mater.* **4** 776–81

Li P N, Lei, Y., Zhong Q P and Li X R 2000 A Chinese structural integrity assessment procedure for pressure vessels containing defects *Int. J. Pressure Vessels Piping* **77** 945–52

Lidbury D P G 1984 The significance of residual stresses in relation to the integrity of LWR pressure vessels *Int. J. Pressure Vessels Piping* **17** 197–328

Liu Y N, Yang H, Liu Y, Jiang B H, Ding J and Woodward R 2005 Thermally induced fcc ⟨−⟩ hcp martensitic transformation in Co–Ni *Acta Mater.* **53** 3625–34

Lupascu D C and Rodel J 2005 Fatigue in bulk lead zirconate titanate actuator materials: a review *Adv. Eng. Mater.* **7** 882–98

Ma S, Brown D, Bourke M A M, Daymond M R and Majurndar B S 2005 Microstrain evolution during creep of a high volume fraction superalloy *Mater. Sci. Eng.* A **399** 141–53

Macdowell A A, Celestre R S, Tamura N, Spolenak R, Valek B, Brown W L, Bravman J C, Padmore H A, Batterman B W and Patel J R 2001 Submicron x-ray diffraction *Nucl. Instrum. Methods Phys. Res.* A **467–8** 936–43

Martin U, Altenberger I, Scholtes B, Kremmer K and Oettel H 1998 Cyclic deformation and near surface microstructures of normalized shot peened steel SAE 10451 *Mater. Sci. Eng.* A **246** 69–80

Masubuchi K 2003 Residual stresses and distortion in welds *Encyclopedia of Materials: Science and Technology* ed K H J Buschow *et al* (Oxford: Elsevier)

Mathar J 1934 Determination of initial stresses by measuring the deformation around drilled holes *Trans. ASME* **56** 249–54

Matthew B A, Green D J and Glass S J 2003 Fracture behavior of engineered stress profile soda lime silicate glass *J. Non-Cryst. Solids* **321** 10–19

McCarthy J, Pei Z, Becker M and Atteridge D 2000 FIB micromachined submicron thickness cantilevers for the study of thin film properties *Thin Solid Films* **358** 146–51

McElhone M and Rugg D 2005 Experimental evaluation of the fatigue performance of aero-engine fan blade dovetails *AeroMat (Florida)* (Cleveland, OH: ASM)

McGuire P A and Groom J J 1979 computational analysis and experimental evaluation for residual stresses from induction heating *EPRI* Battelle Memorial Institute

Meguid S A, Shagal G, Stranart J C, Liew K M and Ong L S 2005 Relaxation of peening residual stresses due to cyclic thermo-mechanical overload *J. Eng. Mater. Technol.—Trans. ASME* **127** 170–8

Michaleris P and Sun X 1997 Finite element analysis of thermal tensioning techniques mitigating weld buckling distortion *Weld. J.* **76** 451s–7s

Milbradt K P 1951 Ring method determination of residual stresses *Proc. Soc. Exp. Stress Anal.* **9** 63–74

Miller K J 2003 Structural integrity—whose responsibility? *Proc. Inst. Mech. Eng. Part L—J. Mater.-Des. Appl.* **217** 1–21

Milne I, Ainsworth R A, Dowling A R and Stewart A T 1988 Assessment of the integrity of structures containing defects *Int. J. Pressure Vessels Piping* **32** 3–104

Minkevich A A, Gailhanou M, Micha J-S, Charlet B, Chamard V and Thomas O 2007 Inversion of the diffraction pattern from an inhomogeouly strained crystal using an iterative algorithm *Phys. Rev.* B **76** 104106

Mollis S E and Clarke D R 1990 Measurement of stresses using fluorescence in an optical microprobe: stresses around indentations in a chromium-doped sapphire *J. Am. Ceram. Soc.* **73** 3189–94

Moore M G and Evans W P 1958 Mathematical correction for stress in removed layers in x-ray diffraction residual stress analysis *SAE Trans.* **66** 340–5

Mori T and Withers P J 2001 Residual stresses: interphase stresses *Encyclopedia of Materials: Science and Technology* ed K H J Buschow (Oxford: Elsevier)

Munsi A, Waddell A J and Walker C A 2001a The effect of vibratory stress on the welding microstructure and residual stress distribution *Proc. Inst. Mech. Eng.* L **215** 99–111

Munsi A, Waddell A J and Walker C A 2001b Modification of residual stress by post-weld vibration *Mater. Sci. Technol.* **17** 601–5

Munsi A S M Y, Waddell A J and Walker C A 2001c Vibratory stress relief—an investigation of the torsional stress effect in welded shafts *J. Strain Anal.* **36** 453–65

Mura T 1987 *Micromechanics of Defects in Solids* (The Hague: Nijhoff)

Narayanaswamy O S and Gardon R 1969 Calculation of residual stresses in glass *J. Am. Ceram. Soc.* **52** 554–8

Newey C W A and Weaver G H 1990 *Materials Principles and Practice* (London: Open University, Butterworths)

Newnham R E 1998 Phase transformations in smart materials *Acta Crystallogr.* A **54** 729–37

Nicholas E D and Thomas W M 1998 A review of friction processes for aerospace applications *Int. J. Mater. Product Technol.* **13** 45–55

Nikitin I, Scholtes B, Maier H J and Altenberger I 2004 High temperature fatigue behavior and residual stress stability of laser-shock peened and deep rolled austenitic steel AISI 304 *Scr. Mater.* **50** 1345–50

Nishioka K, Hanabusa T and Fujiwara H 1974 Theory of x-ray residual stress analysis *Scr. Metall.* **8** 1349–50

Nowell D 1999 Strain changes caused by finite width slots, with particular reference to residual stress measurement *J. Strain Anal. Eng. Des.* **34** 285–94

Noyan I C and Cohen J B 1985 An x-ray diffraction study of the residual stress–strain distributions in shotpeened two-phase brass *Mater. Sci. Eng.* **75** 179–93

Noyan I C and Cohen J B 1987 *Residual Stress—Measurement by Diffraction and Interpretation* (New York: Springer)

Nye J F 1985 *Physical Properties of Crystals—Their Representation by Tensors and Matrices* (Oxford: Clarendon)

Oliver E C, Mori T, Daymond M R and Withers P J 2005 Orientation dependence of martensite variants during loading of Fe–Pd shape memory alloy *Scr. Mater.* **53** 609–12

Oliver E C, Withers P J, Daymond M R, Ueta S and Mori T 2002 Neutron-diffraction study of stress-induced martensitic transformation in TRIP steel *Appl. Phys.* A **74** S1143–5

Orowan E 1948 Fracture and strength of solids *Rep. Prog. Phys.* **12** 185–232

Pang J W L, Holden T M, Turner P A and Mason T E 1999 Intergranular stresses in Zircaloy-2 with rod texture *Acta Mater.* **47** 373–83

Pao Y H, Sachse W and Fukuoka H 1984 Acoustoelasticity and ultrasonic measurements of residual-stresses *Phys. Acoust.* **17** 61–143

Paris P and Erdogan F 1963 A critical analysis of crack propagation laws *J. Basic Eng.* **85** 528–34

Patterson E 2001 Photoelasticity *Encyclopedia of Materials: Science and Technology* ed K H J Buschow *et al* (Oxford: Elsevier)

Peel M, Steuwer A, Preuss M and Withers P J 2003 Microstructure, mechanical properties and residual stresses as a function of welding speed in aluminium AA5083 friction stir welds *Acta Mater.* **51** 4791–801

Pfeifer M A, Williams G J, Vartanyants I A, Harder R and Robinson I K 2006 Three-dimensional mapping of a deformation field inside a nanocrystal *Nature* **442** 63–6

Pintschovius L and Jung V 1983 Residual stress measurements by means of neutron diffraction *Mater. Sci. Eng.* **61** 43–50

Pintschovius L, Jung V, Macherauch E, Schäfer R and Vöhringer O 1981 Determination of residual stress distributions in the interior of technical parts by means of neutron diffraction *Residual Stress and Stress Relaxation; Proceedings of the 28th Army Materials Research Conf.* (*Lake Placid, July*) ed E Kula and V Weiss (New York: Plenum)

Preuss M, Pang J W L, Withers P J and Baxter G J 2002 Inertia welding nickel-based superalloy: II: Residual stress development *Metal. Mater. Trans.* A **33** 3227–34

Prevéy P, Jayaraman N, Ontko N, Shepard M, Ware R and Coate J 2005 *Mechanical Suppression of SCC and Corrosion Fatigue In 300M Steel Landing Gear (Lambda Technologies)*

Prevey P S 2000 The effect of cold work on the thermal stability of residual compression in surface enhanced IN718 *20th ASM Materials Solution Conf. (St Louis, MI)*

Prevey P S and Cammett J T 2004 The influence of surface enhancement by low plasticity on the corrosion fatigue performance of AA7075: I. *J. Fatigue* **24** 975–82

Prevey P S, Shepard M J and Smith P R 2001 The effect of low plasticity burnishing LPB on the HCF performance and FOD resistance of Ti–6Al–4V *6th National Turbine Engine HCF Conf. (Jacksonville, FL)*

Prime M 1999 Residual stress measurement by successive extension of a slot: the crack compliance method *Appl. Mech. Rev.* **52** 75–96

Prime M 2000 The contour method; simple 2D mapping of residual stresses *Int. Conf. Res. Stress 6* ed G A Webster (Oxford: Institute of Materials)

Prime M B 2001 Cross sectional mapping of stresses by measuring the contour after a cut *J. Mater. Eng. Technol.— Trans. ASME* **123** 162–8

Prime M B and Hill M R 2002 Residual stress, stress relief and inhomogeneity in Al plate *Scr. Mater.* **46** 77–82

Prime M B and Hill M R 2004 Measurement of fiber-scale residual stress variation in a metal-matrix composite *J. Compos. Mater.* **38** 2079–95

Pugh S F 1958 The mechanism of growth of uranium on thermal cycling in the alpha-range *J. Inst. Met.* **86** 497–503

Quinn S, Dulieu-Barton J M and Langlands J M 2004 Progress in thermoelastic residual stress measurement *Strain* **40** 127–33

Rankin J E, Hill M R and Hackel L A 2003 The effects of process variations on residual stress in laser 7049 T73 aluminum alloy *Mater. Sci. Eng.* A **349** 279–91

Rendler N J and Vigness I 1966 Hole-drilling strain-gage method of measuring residual stresses *Exp. Mech.* **6** 577–86

Retraint D and Lu J 2000 Study of residual stress distribution by the combination of three techniques in an aluminium based MMC *ECRS 5: Proc. 5th European Conf. on Residual Stresses Mater. Sci. Forum* **347–9** 498–503

Reynolds A P, Tang W, Gnaupel-Herold T and Prask H 2003 Structure, properties, and residual stress of 304L stainless steel friction stir welds *Scr. Mater.* **48** 1289–94

Rice J R 1968 A path independent integral and the approximate analysis of strain concentration by notches and cracks *J. Appl. Mech.* **35** 379–86

Richards D G, Prangnell P B, Withers P J, Williams S W, Wescott A and Oliver E C 2006 Geometry effects when controlling residual stresses welds by mechanical tensioning *ECRS7 Mater. Sci. Forum* **524–5** 71–6

Roche R L 1989 Practical procedure for stress classification *Int. J. Pressure Vessels Piping* **37** 27–44

Roylance D 1996 *Mechanics of Materials* (New York: Wiley)

Ruschau J J, John R, Thompson S R and Nicholas T 1999 Fatigue crack nucleation and growth rate behavior of laser shock peened titanium: I. *J. Fatigue* **21** S199–209

Sabate N, Vogel D, Gollhardt A, Keller J, Michel B, Cane C, Gracia I and Morante J R 2006 Measurement of residual stresses in micromachined structures in a microregion *Appl. Phys. Lett.* **88** 254–9

Sadanada K, Vasudevan A K, Holtz R L and Lee E U 1999 Analysis of overload effects and related phenomena: I. *J. Fatigue* **21** S233–46

Said G 2006 Study on ASTM E399 and ASTM E1921 standards *Fatigue Fract. Eng. Mater. Struct.* **29** 606–14

Saigal A, Kupperman D S and Majumdar S 1992 Residual strains in titanium matrix high temperature composites *Mater. Sci. Eng.* A **150** 59–66

Sauer G 1964 Stretching as a method to reduce residual stresses of 1st step *Z. Metallk.* **55** 811–15

Schajer G S 1981 Application of finite element calculations to residual stress measurements *J. Eng. Mater. Technol.* **103** 157–63

Schajer G S 1988 Measurement of non-uniform residual stresses using the hole-drilling method (part I) *J. Eng. Mater. Technol.* **103** 338–43

Schajer G S 1988 Measurement of non-uniform residual stresses using the hole-drilling method (part II) *J. Eng. Mater. Technol.* **103** 344–9

Schajer G S 2001 Residual stresses: destructive measurements *Encyclopedia of Materials Science and Technology* ed K H J Buschow *et al* (Oxford: Elsevier)

Schoenig F C, Soules J A, Chang H and Dicello J J 1995 Eddy current measurement of residual stresses induced by shot peening in titanium Ti–6Al–4V *Mater. Eval.* **53** 22–6

Sendek P 1997 Vibration treatment—effective method of improving the dimensional stability of welded structures: investigation and prectice *Weld. Surf. Rev.* **8** 221–8

Shih C F and Hutchinson J W 1976 Fully plastic solitions and large-scale yielding estimates for plane stress crack problems *J. Eng. Mater. Technol., Trans. ASME* **98** 289–95

Sinclair R, Preuss M and Withers P J 2005 Imaging and strain mapping fibre by fibre in the vicinity of a fatigue crack in a Ti/SiC fibre composite *Mater. Sci. Technol.* **21** 27–34

Smith D J and Garwood S J 1990 The significance of prior overload on fracture-resistance—a critical-review *Int. J. Pressure Vessels Piping* **41** 255–96

Stacey A, Barthelemy J Y, Leggatt R H and Ainsworth R A 2000 Incorporation of residual stresses into the SINTAP defect assessment procedure *Eng. Fract. Mech.* **67** 573–611

Staron P, Kocak M and Williams S 2002 Residual stresses in friction stir welded Al sheets *Appl. Phys.* A **74** S1161–2

Stefanescu D, Steuwer A, Owen R A, Nadri B, Edwards L, Fitzpatrick M E and Withers P J 2004 Elastic strains around cracked cold expanded fastener holes measured using the synchrotron x-ray diffraction technique *J. Strain Anal.* **39** 459–69

Steuwer A, Peel M and Withers P J 2006 Dissimilar friction stir welds in AA5083-AA6082. The effect of processing parameters on residual stress *Mater. Sci. Eng.* A **441** 187–96

Steuwer A, Rahman M, Fitzpatrick M E, Edwards L and Withers P J 2007 The evolution of residual and crack-tip stresses during a fatigue overload *Acta Mater.* submitted

Stone H J, Bhadeshia H K D H and Withers P J 2008 In situ monitoring of weld transformations to control weld residual stresses *MecaSENS Conf. (Austria, 2007) Mater. Sci. Forum* submitted

Suresh S 1983 Mechanisms of fatigue crack growth retardation following overloads *Eng. Fract. Mech.* **18** 577–93

Suresh S 1991 *Fatigue of Materials* (Cambridge: Cambridge University Press)

Suresh S and Ritchie R O 1984 Propagation of short fatigue cracks *Int. Met. Rev.* **29** 445–76

Tada H 1970 Westergaard stress functions for several periodic crack problems *Eng. Fract. Mech.* **2** 177–80

Tada H, Paris P and Irwin G 1985 *The Stress Analysis of Cracks Handbook* (St Louis, MO: Del Research Corporation)

Thomas W M, Nicholas E D, Needham J C, Murch M G, Temple-Smith P and Dawes C J 1991 Friction stir butt welding *International Patent Specification* PCT/GB92/02203; *GB Patent Specification* 9125978.8; *US Patent Specification* 5460317

Tiitto S 1977 Influence of microstructure on magnetization transitions in steel *Acta Polytech. Scand.—Appl. Phys. Ser.* **119** 3–80

Timoshenko S P and Goodier J N 1982 *Theory of Elasticity* (New York: McGraw-Hill)

Tomé C 2001 Elastic behaviour of polycrystals *Encyclopedia of Materials: Science and Technology* ed K H J Buschow (Oxford: Elsevier)

Turski M, Spindler M W, Bouchard P J and Withers P J 2007 Residual stress driven creep cracking in type 316 stainless steel *Acta Mater.* submitted

Ueda Y and Yuan M G 1993 Prediction of residual-stresses in butt welded plates using inherent strains *J. Eng. Mater. Technol.—Trans. ASME* **115** 417–23

Vaidyanathan R, Bourke M A M and Dunand D C 1999 Phase fraction, texture and strain evolution in superelastic NiTi and NiTi-TiC composites investigated by neutron diffraction *Acta Mater.* **47** 3353–66

Vaidyanathan S and Finnie I 1971 Determination of residual stresses from stress intensity factor measurements *J. Basic Eng.* **93** 242–6

Van Humbeeck J 1999 Non-medical applications of shape memory alloys *Mater. Sci. Eng.* A **275** 134–48

Vasudevan A K and Sadanada K 1995 Classification of fatigue crack growth behavior *Met Trans.* A **26** 1221–34

Vasudevan A K, Sadanada K and Glinka G 2001 Critical parameters for fatigue: I. *J. Fatigue* **23** S39–53

Vishay Measurements Group 1993 *Measurement of Residual Stresses by the Hole drilling Strain Gauge Method*

Walker C A, Waddell A J and Johnston D J 1995 Vibratory stress relief—an investigation of the underlying processes *Proc. Inst. Mech. Eng.* E **209** 51–8

Wanjara P and Jahazi M 2005 Linear friction welding of Ti–6Al–4V: processing, microstructure, and mechanical-property inter-relationships *Metall. Mater. Trans.* A **36** 2149–64

Watts M R and Withers P J 1997 The interpretation of x-ray stress measurements of metal matrix composites using computer modelling techniques *11th Int. Conf on Composite Materials* (*Gold Coast, Australia*) ed M L Scott *et al* (Cambridge, UK: Woodhead Publishing)

Webster G A and Ezeilo A N 2001 Residual stress distributions and their influence on fatigue lifetimes *Int. J. Fatigue* **23** S375–83

Webster P J, Wang X D and Mills G 1996 Through thickness strain scanning using synchrotron radiation *Mater. Sci. Forum* **228** 227–32

Westergaard H M 1939 Bearing pressures and cracks *Trans. ASME* **61** A49–53

Wheeler O E 1972 Spectrum loading and crack growth *J. Basic Eng.* **94** 181–6

Wilson D V and Konnan Y A 1964 Work hardening of a steel containing a coarse dispersion of cementite particles *Acta Metall.* **12** 617–28

Withers P J 1988 The development of the Eshelby model and its application to metal matrix composites *PhD Thesis* University of Cambridge

Withers P J 1995 Neutron strain measurement of internal strain in metal and ceramic composites *Key Eng. Mater.* **108–10** 291–314

Withers P J 2003 Use of synchrotron x-ray radiation for stress measurement *Analysis of Residual Stress by Diffraction using Neutron and Synchrotron Radiation* ed M E Fitzpatrick and A Lodini (London: Taylor and Francis)

Withers P J and Bhadeshia H K D H 2001 Residual stress: II. Nature and origins *Mater. Sci. Technol.* **17** 366–75

Withers P J and Clarke A P 1998 A neutron diffraction study of load partitioning in continuous Ti/SiC composites *Acta Mater.* **46** 6585–98

Withers P J, Jensen D J, Lilholt H and Stobbs W M 1987 The evaluation of internal stresses in a short fibre metal matrix composite by neutron diffraction *Proc. ICCM VI/ECCM2 (London)* ed F L Matthews (Oxford: Elsevier)

Withers P J, Preuss M, Steuwer A and Pang J W L 2007 Methods for the obtaining the strain-free lattice parameter when using diffraction to determine residual stress *J. Appl. Crystallogr.* **40** 891–904

Withers P J, Stobbs W M and Pedersen O B 1989 The application of the eshelby method of internal stress determination for short fibre metal matrix composites *Acta Met.* **37** 3061–84

Withers P J and Webster P J 2001 Neutron and synchrotron x-ray strain scanning *Strain* **37** 19–31

Wöhler A 1860 Versuche zur Ermittlung der auf die Eisenbahnwagenachsen einwirkenden Kräfte und die Widerstandsfähigkeit der Wagen-Achsen *Z. Bauwesen* **X** 583–616

Wong A K 2001 Stress distribution: analysis using thermoelastic effect *Encyclopedia of Materials: Science and Technology* ed K H J Buschow *et al* (Oxford: Elsevier)

Wu S, Zhao H Y, Lu A L, Fang H Z and Tang F 2003 A micro-mechanism model of residual stress reduction by low frequency alternating magnetic field treatment *J. Mater. Process. Technol.* **132** 198–202

Yamamoto J, Muramatsu Y, Zenitani S, Hayakawa N and Hiraoka K 2002 Control of welding residual stress by low-temperature transformation welding consumables—influence of restraint of joint and transformation-temperature on residual stress *Proc. 6th Int. Conf. on Trends in Welding Research (Pine Mountain)* pp 902–5

Yang Y P, Dong P, Tian X and Zhang Z 1998 Prevention of hot cracking of high strength aluminum alloy by mechanical rolling *Proc. 5th Int. Conf. Trends in Welding Research (Pine Mountain)*

Yang Y P, Dong P, Zhang J and Tian X 2000 A hot-cracking mitigation technique for welding high-strength aluminum alloy *Weld. J.* **79** 9S–17S

Young R J 2001 Residual stresses: measurement by Raman shifts *Encyclopedia of Materials: Science and Technology* ed K H J Buschow *et al* (Oxford: Elsevier)

Zacharia T, Vitek J M, Goldak J A, Debroy T A, Rappaz M and Bhadeshia H 1995 Modeling of fundamental phenomena in welds *Modelling Simul. Mater. Sci. Eng.* **3** 265–88

Zhuang W Z and Halford G R 2001 Investigation of residual stress relaxation under cyclic stress *Int. J. Fatigue* **23** S31–37

Zien H M 1983 Fracture-mechanics J-integral calculations in thermo-elasto-plasticity *Comput. Struct.* **17** 775–81

Zrnik J, Muransky O, Lukas P, Sittner P and Novy Z 2005 In-situ neutron diffraction analysis of phase transformation kinetics in TRIP steel *New Frontiers of Processing and Engineering in Advanced Materials Mater. Sci. Forum* **502** 339–44